Precambrian Research 410 (2024) 107474

Contents lists available at ScienceDirect

Precambrian Research

journal homepage: www.elsevier.com/locate/precamres

Boron sources of tourmaline-rich Nb-Y-F-pegmatites in south Norway: Implications for pegmatite melt origin

Erika De La Cruz [a], Axel Müller [a,b,*], Robert B. Trumbull [c], Pedro Faria [a], Tom Andersen [a,d], Muriel Erambert [e], Magnus Kristoffersen [e]

[a] Natural History Museum, P.O. 1172 Blindern, N-0318 Oslo, Norway
[b] Natural History Museum, Cromwell Road, London SW7 5BD, UK
[c] GFZ German Research Centre for Geosciences, Telegrafenberg, 14473 Potsdam, Germany
[d] Department of Geology, University of Johannesburg, PO Box 524, Auckland Park, 2006, Johannesburg, South Africa
[e] University of Oslo, Department of Geosciences, P.O. Box 1047 Blindern, 0316 Oslo, Norway

ARTICLE INFO

Keywords:
Tourmaline
Pegmatite
Boron isotopes
Sveconorwegian
Bamble
Kongsberg
Idefjorden

ABSTRACT

Tourmaline is common in rare element pegmatites of the Nb-Y-F (NYF) type in the south-central part of the Proterozoic Sveconorwegian orogen in southern Norway. In the global context, however, tourmaline appears rare in this type of pegmatite. This study aims to explain the unusual tourmaline abundance in these pegmatites and the origin of boron (B) in the respective melts, and to raise awareness of tourmaline in NYF pegmatites generally. Tourmalines from six pegmatites in three Sveconorwegian lithotectonic units: Bamble, Kongsberg and Idefjorden, were investigated in terms of their mineral chemistry and $\delta^{11}B$ values, in addition to bulk rock analyses of pegmatites and host rocks. Tourmalines in pegmatites from Bamble and Kongsberg record B isotopic compositions ($\delta^{11}B$ = -1.0 to + 9.9 ‰) that are heavy relative to continental crust and mantle sources. In contrast, tourmaline in pegmatites and host rocks from Idefjorden have light B isotopic ratios (δ11B = -14.8 to −12.5 ‰) that are typical crustal values. We suggest that the latter melts were sourced from orthogneisses at depth. We relate the heavy B isotopic composition of Bamble and Kongsberg pegmatites to regional Na-metasomatism by fluids sourced from Mesoproterozoic shallow marine sediments. This is supported by previously published $\delta^{11}B$ ratios from metasomatized Bamble host rocks. The spatial association of pegmatites with Na-metasomatism in the basement rocks suggests that metasomatism enhanced the fertility and B-concentration in the affected lithologies, favouring partial melting and the formation of tourmaline-bearing pegmatites.

These findings contribute to understanding the petrogenesis of Sveconorwegian pegmatites but they also imply that B can play a greater role in the formation of NYF pegmatites than previously thought and that tourmaline has value as a petrogenetic tool in this type of pegmatites as well as in the Li-Cs-Ta (LCT) type to which is it is more commonly applied.

1. Introduction

Tourmaline is the most common borosilicate mineral in the Earth's crust. It is a complex mineral supergroup with numerous chemical end-members (e.g. Henry et al., 2011) and its chemical composition depends on the geological setting. Brown, Mg-rich dravite and the commonly green, Ca-rich Uvite, for example, occur mainly in metamorphic environments, while black, Fe-rich schorl is common in granitic rocks, and the Li-rich elbaite, which can be green, red to pink, blue, orange, yellow or colorless, is primarily found in granitic pegmatites. Because the tourmaline is the main mineral host for boron in most rocks and boron is partitioned preferentially into fluid or melt phases (Brenan et al., 1998), the chemical composition and the boron isotopic signature of tourmaline are increasingly used to trace origins, pathways, and interactions of tourmaline-forming aqueous fluids and/or melts related to orogenic processes and ore formation (e.g. Marschall et al., 2009; Van Hinsberg et al., 2011a, b; Palmer, 2017; De Hoog and Savov, 2018; Trumbull and Slack, 2018).

An important aspect of boron isotope geochemistry is the fractionation of the two stable isotopes ^{11}B and ^{10}B between coexisting phases,

* Corresponding author.
E-mail address: a.b.muller@nhm.uio.no (A. Müller).

https://doi.org/10.1016/j.precamres.2024.107474
Received 6 January 2024; Received in revised form 4 June 2024; Accepted 6 June 2024
Available online 13 June 2024

which depends on the coordination environment of boron in each phase (^{11}B favoring trigonal sites vs. ^{10}B in tetrahedral sites) and is inversely related to temperature. For example, boron in sheet silicates is in tetrahedral coordination while trigonal coordination dominates in neutral to acidic fluids (Sanchez-Valle et al., 2005; Kowalski and Wunder, 2018). Thus, aqueous fluids have a preference for the heavy isotope ^{11}B and consequently, metamorphic dehydration reactions lead to successively lower δ^{11}B values in the higher-grade rocks (Moran et al., 1992; Marschall et al., 2007; Meyer et al., 2008; Konrad-Schmolke and Halama, 2014). The fractionation factor between fluid and white mica is about 15 permil at 300 °C and 8 permil at 600 °C (Kowalski and Wunder, 2018). Boron in tourmaline is in trigonal coordination and the tourmaline-fluid fractionation factor is much lower than for mica: about 4 permil at 300 °C and 1.3 permil at 600 °C (Meyer et al., 2008). Experimental B-isotope fractionation between hydrous granitic melts and tourmaline (Cheng et al., 2022) revealed about 1 permil

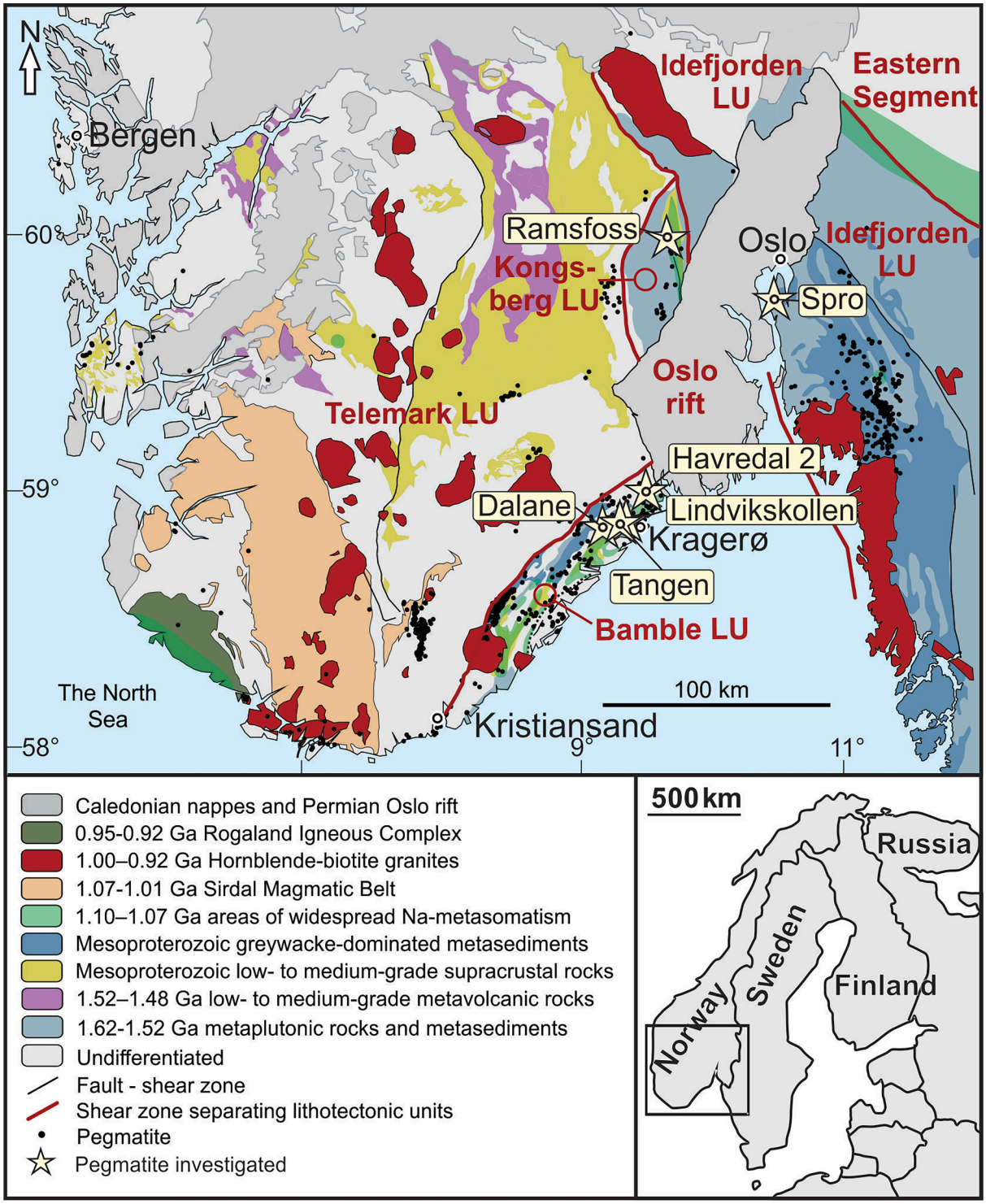

Fig. 1. Simplified map of the Sveconorwegian orogen of southern Norway and southwestern Sweden. Note that the areas of widespread Na-metasomatism (light green) correspond approximately to the location of pegmatites fields in the Bamble and Kongsberg lithotectonic units (LU). Modified from Rosing-Schow et al. (2023). Geodetic datum used is UTM.

fractionation at 660 °C and 0.3 permil at 800 °C. Therefore, while in general the B-isotope ratio of tourmaline is not the same as the fluid or melt from which it formed, at magmatic temperatures the difference is small and the B isotopic signature of magmatic tourmalines offers direct information about melt sources (see also Barth, 1993; Marschall and Jiang, 2011).

Tourmaline is a peraluminous mineral and it forms a common constituent in the Li-Cs-Ta (LCT) family of granitic pegmatites. The LCT pegmatites are characterized by enrichments in Li, Cs, Rb, Be and Ta and are considered to be associated with peraluminous granitic bodies formed by melting of (meta)sedimentary crustal material (Černý et al., 2012). However, LCT pegmatites are not always found within or close to a granitic pluton, and in some cases, there is no evidence of a parental granite and the pegmatites are considered to be anatectic, having formed directly by partial melting of suitable source rocks (e.g. Simmons et al., 2016; Knoll et al., 2023). The boron content in the metasedimentary source rocks of LCT pegmatites is relatively high because of the abundance of mica (Trumbull and Slack, 2018). In contrast, tourmaline is generally rare in the Nb-Y-F (NYF) pegmatite family (but see below). The NYF pegmatites are characterized by enrichments in Nb, Ti, Y, rare earth elements (REE), Zr, U, Th and F and are considered to be typically associated with metaluminous to alkaline (locally peralkaline) granitic bodies or to anatexis of intermediate to mafic rocks (Wise, 1999; Černý et al., 2012; Müller et al., 2015, 2017, Shaw et al., 2016; Rosing-Schow et al., 2023). These source rocks are typically B-poor compared to the average B content of the Earth's crust of 17 ppm (Rudnick and Gao, 2003).

Contrary to expectation, tourmaline is relatively common in the Mesoproterozoic NYF pegmatites of the Bamble and Kongsberg areas of the Sveconorwegian orogen in southern Norway. Other examples of NYF pegmatites with tourmaline have recently been described worldwide (Bohemian Massif, Czech Republic: Novák et al., 2011; Oslo Rift, Norway: Sunde et al., 2020; Sierra de San Luis, Argentina: Ribacki et al., 2022) and they may be more common than once believed. These occurrences raise important general questions about B sources and B enrichment in this economically important family of pegmatites and this has motivated the present study.

We present data on the major- and trace-element composition as well as the B isotopic ratios of tourmaline from rare-element pegmatites from different parts of the Sveconorwegian orogen. Recent studies have suggested that most of the Sveconorwegian rare-element pegmatites derived from partial melting (anatexis) of their host rocks rather than fractionation of a parental granite (Müller et al., 2015, 2017, Rosing-Schow et al., 2023). Indeed, within our study areas of Bamble, Modum and Nesodden most tourmaline-bearing NYF pegmatites occur where no coeval granite pluton is exposed (Fig. 1). By constraining the B source in the Sveconorwegian NYF pegmatites with complementary whole rock and mineral chemistry data, this tourmaline study can also shed light on the idea of an anatectic origin for the pegmatite melts.

2. Geological setting

The Sveconorwegian orogen (1140 to 920 Ma) comprises the southwest margin of Fennoscandia and includes areas in southwest Sweden and southern Norway (Fig. 1). The orogen formed through a series of geodynamic processes including subduction, arc-continent collision, and continent–continent collision at the western margin of Baltica leading to the formation of the supercontinent Rodinia. However, the exact geometry and collisional history of the paleocontinents involved in the orogeny are still debated (e.g., Slagstad et al., 2020; Bingen et al., 2021). Metamorphic rocks with protolith ages of 1900 to 1400 Ma are well documented this part of Fennoscandia (Andersen, 1997; Andersen et al., 2001, 2004; De Haas et al., 1993; Knudsen et al., 1997; Möller et al., 2015; Roberts et al., 2013). Voluminous A- and I-type granites and minor gabbros, mafic dykes and anorthosites intruded various parts of the orogen between 1235 and 920 Ma (e.g., Söderlund et al., 2005; Andersen et al., 2007; Van der Auwera et al., 2011; Slagstad et al., 2012; Høy, 2016; Jensen and Corfu, 2016; Granseth et al., 2020). Geotectonically, the orogen is composed of sub-domains separated by crustal scale shear zones, the definition, nomenclature, and significance of which remain controversial (e.g., Andersen, 2005; Bingen et al., 2008; Slagstad et al., 2017, 2020; Bingen et al., 2021). For the present study, we apply the nomenclature according to the Geological Survey of Norway (Torgersen et al., 2021). Consistent with this scheme, we refer to the Eastern Segment and the Idefjorden, Kongsberg, Bamble, and Telemark lithotectonic units (lithotectonic unit is abbreviated as LU in the following; Fig. 1).

The majority of studied pegmatites (Lindvikskollen, Tangen, Havredal, Dalane) belong to the Kragerø pegmatite field located near Kragerø in the *Bamble LU* (Table 1). The *Bamble LU* is approximately 30 km wide and 135 km long and predominantly consists of migmatitic, granitic para- and orthogneisses, with protolith ages between 1600 and 1520 Ma (e.g., Andersen et al., 2004), quartz-rich metasedimentary rocks deposited in shallow marine environments between 1500 and 1400 Ma (Starmer, 1985; Andersen et al., 1995; Andersen and Knudsen, 1996; Knudsen et al., 1997; De Haas et al., 1999), and intrusive felsic and mafic magmatic rocks emplaced between 1235 and 1135 Ma (e.g., Heaman and Smalley, 1994). All these rocks were reworked during the Sveconorwegian orogeny resulting in two amphibolite- to granulite-facies metamorphic peaks, at 1140 to 1125 Ma and at 1110 to 1080 Ma (Bingen et al., 2008). During the second high-grade regional metamorphism, lithologies in the *Bamble LU* were affected by widespread Na-metasomatism (scapolitization and albitization) between 1110 and 1070 Ma (e.g., Lieftink et al., 1994; Nijland and Touret, 2001; Engvik et al., 2009, 2011, 2017). Scapolitization especially affected metagabbros (Nijland et al., 2014) while subsequent albitization affected both metagabbros and metasediments in the central and northeastern parts of the *Bamble LU* (Bugge, 1965; Elliott, 1966; Engvik et al., 2008, 2018; Nijland and Touret, 2001; Fig. 1). At Lindvikskollen, albitization of host rocks next to the investigated pegmatite was dated at 1090 and 1084 Ma (Engvik et al., 2011). Metasomatism was closely followed by the formation of granitic rare element pegmatites throughout the *Bamble LU* between 1100 and 1030 Ma (Rosing-Schow et al., 2023). U-Pb columbite dating of the studied Tangen pegmatite revealed a crystallization age of 1082 ± 4 Ma (Müller et al., 2017). In the Kragerø area, pegmatites are commonly emplaced into metagabbros and metasomatic scapolites and albitites. Albitites are almost monomineralic albite rocks with minor titanite, rutile, apatite, and tourmaline. This suite of metagabbros has a crystallization age of 1149 ± 7 Ma (U-Pb zircon age of the Ødegården metagabbro, part of the suite located close to the investigated Havredal pegmatite; Engvik et al., 2011).

The *Kongsberg LU*, which hosts the studied Ramfoss pegmatite, is characterised by N-S trending metaigneous and quartzite-rich metasedimentary sequences. The onset of sedimentation of quartzites of the Modum Complex, the host rocks of the Ramfoss pegmatite, was at 1434 ± 29 Ma (Andersen and Grorud, 1998). The metasedimentary sequences were intruded by gabbros at 1224 ± 15 Ma (Munz et al., 1994). Later, during the Sveconorwegian orogeny, they were subjected to upper amphibolite facies metamorphism and synorogenic Na-metasomatism (albitization) at 1080 ± 3 Ma (Munz et al., 1994). Widespread Na-metasomtism occurred particularly in the Modum area where most of the larger gabbro bodies and the investigated Ramfoss pegmatite are located (Jøsang, 1966; Munz et al., 1994; Munz et al., 1995). The crystallization age of the Ramfoss pegmatite is 1045 ± 12 Ma (Pb-Pb albite–titanite–turmaline–apatite isochron; Andersen and Grorud, 1998), postdating the albitization event.

The *Idefjorden LU*, where the investigated Spro pegmatite is located, consists of mainly calc-alkaline and tholeiitic igneous rocks (1660 to 1520 Ma), associated with greywacke-bearing metasedimentary sequences (Bingen et al., 2001; Åhäll and Connelly, 2008). The protolith ages of the amphibolitic host rocks of the Spro pegmatite range from 1900 to 1600 Ma (Jacobsen and Heier, 1978; Pedersen, 1978; Skiöld,

Table 1
Investigated pegmatites, the pegmatite district/field and tectonic unit to which they belong, host rocks and age of emplacement. Ages of the Lindvikskollen, Havredal, and Dalane pegmatites have not been determined (n.d.) but it is assumed that they belong to age group 1 (1090–1030 Ma) according to Rosing-Schow et al. (2022; see also text).

Pegmatite locality	Pegmatite district/ field	Tectono-metamorphic host unit	Main minerals	Indicative accessories	Pegmatite zoning	Outcropping pegmatite size	Host rocks	Crystallization age
Lindvikskollen	Bamble district/ Kragerø field	Bamble Sector	K-feldspar, plagioclase, quartz and biotite	Allanite-(Ce), euxenite-(Y), fluorapatite, hellandite-(Y), schorl	Distinct simple zoned with multiple quartz cores	500 x 200 m	Metagabbro, Albitite	n.d. 1090–1030 Ma[1]
Tangen	Bamble district, Kragerø field	Bamble Sector	Albite (var. ‘ cleavelandite’), K-feldspar, quartz	Allanite-(Ce), fluorapatite, phenakite, columbite (Fe,Mn), topaz, schorl	Distinct simple zoned	40 x 15 m	Metagabbro	1082 ± 4.5 Ma[2]
Havredal	Bamble district, Kragerø field	Bamble Sector	K-feldspar, plagioclase, quartz, muscovite	Schorl, hematite	Weakly simple zoned	100 x 15 m	Migmatitic gneiss, metagabbro	n.d. 1090–1030 Ma[1]
Dalane	Bamble district, Kragerø field	Bamble Sector	K-feldspar, plagioclase, quartz, biotite, muscovite	Allanite-(Ce), fergusonite-(Y), garnet, beryl, schorl	Weakly simple zoned	50 x 6 m	Migmatitic gneiss, amphibolite gneiss	n.d. 1090–1030 Ma[1]
Ramfoss	Kongsberg-Modum district	Kongsberg Sector	K-feldspar, oligoclase, albite, quartz, muscovite	Allanite (Y), schorl, titanite	Weakly simple zoned	15 x 6 m	Quartzite	1045 ± 12 Ma[3]
Spro	Østfold-Halland district	Idefjorden ‘Terrane’	K-feldspar, quartz, oligoclase, albite, muscovite,	Samarskite-(Y), beryl, topaz, fluorite, schorl	Distinct simple zoned	230 x 25 m	Amphibole gneiss, granite gneiss	1036 ± 2 Ma[2]

Source of ages: [1] Rosing-Schow et al. (2022), [2] Müller et al. (2017), [3] Andersen and Grorud (1998).

1976). The Spro granitic gneiss, the other host rock of the Spro pegmatite, has a crystallization age of 1542 to 1493 Ma (Pózer Bue, 2008). During the Sveconorwegian orogeny these rocks were deformed under amphibolite-facies conditions between at 1037 ± 4 Ma (Narum et al., 2021). Partial melting associated with major shear zones occurred between 1039 to 997 Ma (Viola et al., 2013). The obtained crystallization age of the Spro pegmatite (1036 ± 2 Ma; Rosing-Schow et al., 2023), corresponds to the regional, shear-zone-related partial melting event.

3. Description of the investigated pegmatites

The *Lindvikskollen pegmatite* forms an irregular body about 500 m long in the E-W direction and up to 200 m wide (Fig. 2A; Green, 1956, De la Cruz, 2021). The north contact of the pegmatite to the host rocks dips 15 to 45° to the south and the south contact about 25 to 40° northward (Fig. 2B). The pegmatite was mined for K-feldspar from the end of 19th century until the 1930′s. The pegmatite intruded a massive metagabbro which was scapolitized and albitized at the W/NW contact of the pegmatite at 1090 and 1084 Ma (Engvik et al., 2011). Beside metagabbro, the pegmatite cross-cuts with sharp contacts to the albitites, thus the Na-metasomatism predates pegmatite formation. An up to 8 m wide and approximately 200 m long tourmaline-bearing granite dyke occurs about 150 m NW of the pegmatite (Fig. 2A). The major mineral assemblage of the pegmatite includes K-feldspar, plagioclase (oligoclase), quartz, and biotite (Table 1). Black tourmaline is minor with an abundance of about 1 vol% and crystal sizes up to 80 cm long (Fig. 3A and B). Accessories are muscovite, monazite-(Ce), titanite, magnetite, columbite group minerals, allanite-(Ce), hellandite-(Y), fergusonite-(Y), aeschynite-(Y), euxinite-(Y), zircon, xenotime-(Y), thorite, ilmenite, rutile, gadolinite group minerals, fluorapatite, phenakite, bastnäsite-(Ce), caysichite-(Y), chernovite-(Y), hingganite-(Y) and kainosite-(Y) (Brøgger, 1903; Schei, 1904; Kristiansen, 1993; Larsen, 2008 and own observations). The pegmatite exhibits three principal mineralogical zones with discontinuous and gradual contacts (De la Cruz, 2021). A very coarse-grained, relatively equigranular pegmatitic granite is considered here as the wall zone. The width of the wall zone varies between 5 and 50 m (Fig. 2B). Here, black tourmaline occurs in randomly distributed, isolated crystal clusters (up to 50 cm in diameter) predominantly hosted by quartz in a very coarse matrix of K-feldspar, plagioclase, quartz, and biotite (Fig. 3B). Along the central northern contact, the megacrystic wall zone grades into a medium-grained, equigranular granitic rock (orange areas with dotted patterns in Fig. 2A). This medium-grained facies is considered as part of the wall zone and reaches a thickness of up to 5 m. The wall zone contains at least three core zones formed predominantly of massive quartz, which are up to 20 m in diameter (pink areas Fig. 2A and yellow-pink zone in Fig. 2B). The quartz cores are surrounded by up to 5 m wide intermediate zones (also called blocky zones; Fig. 2B) distinguished from the wall zone by the occurrence of subhedral to euhedral K-feldspar megacrysts up to 2 m in size (Fig. 3C) and up to 2 m large biotite sheets. The intermediate zones also contain quartz, muscovite, and tourmaline. Here black tourmaline forms layers (Fig. 3C) also known as tourmaline “lines” in the literature from *gem*-tourmaline pegmatites (e.g. Roda-Robles et al., 2015).

The *Tangen pegmatite* occurs 1.3 km NW of the Lindvikskollen pegmatite. It is a somewhat irregular body measuring about 40 by 60 m and hosted by amphibolite (Green, 1956; De la Cruz, 2021). The pegmatite shows a relatively well developed zoning consisting of a granitic border zone up to 10 cm wide, and a wall zone about 1 m in thickness which grades into a megacrystic intermediate zone. The centre of the pegmatite is occupied by a massive quartz core about 10 m in diameter with inclusions of cleavelandite (platy albite) and tourmaline. At the core margin, euhedral phenakite crystals up to 20 cm in length have been found. The border zone is the only part of the pegmatite where up to 4 cm large biotite crystals are found. Elsewhere, mica is absent. The wall zone is characterised by abundant magnetite as the major accessory mineral followed by zircon and titanite. The transition from the wall to the intermediate zone is characterised by the loss of magnetite and the appearance of black tourmaline. Typical for the intermediate zone are K-feldspar megacrysts (up to 2 m) surrounded by cleavelandite plates up to 20 cm long. Cleavelandite is the most abundant feldspar variety at Tangen. Tourmaline masses up to 50 cm in size are embedded in cleavelandite. U-Pb ages obtained from columbite-(Mn) from the Tangen pegmatite yielded an age of 1082.3 ± 4.5 Ma

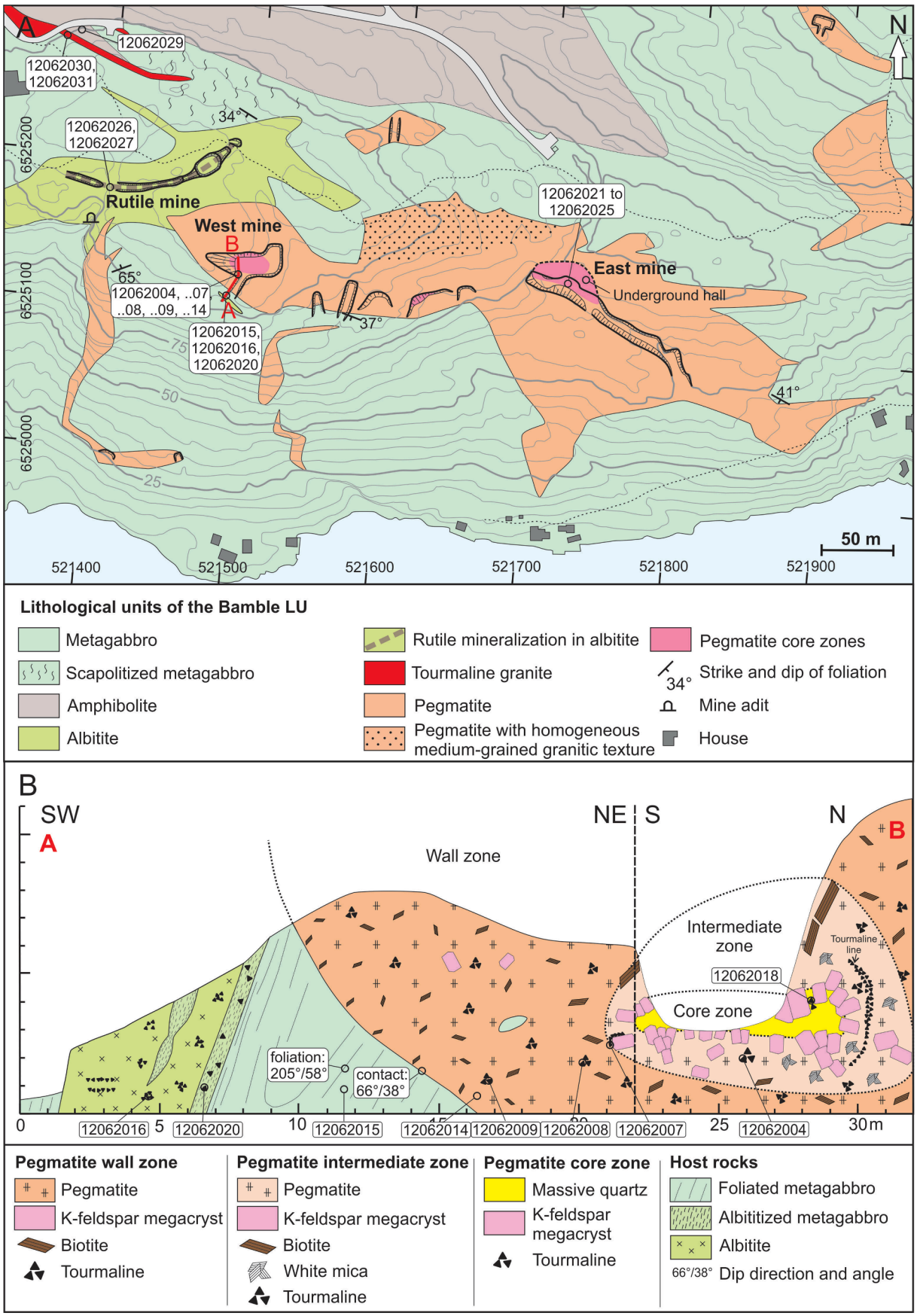

Fig. 2. A – Detailed geological map of the Lindvikskollen pegmatite with sample locations. B – Cross-section of the southwest contact, wall zone, intermediate zone and core of the Lindvikskollen pegmatite with sample locations.

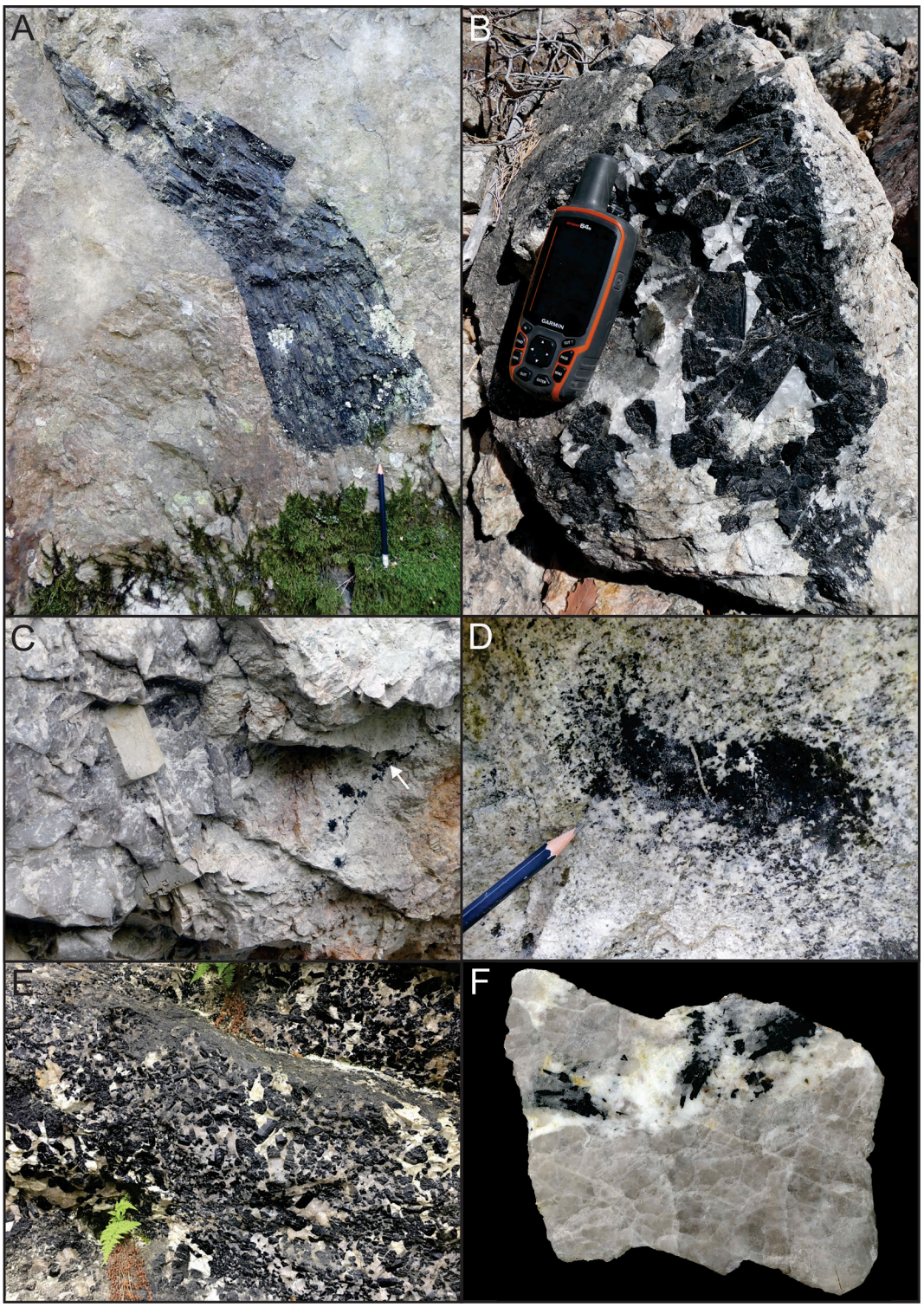

Fig. 3. A – Tourmaline megacryst, 80 cm long, at edge of the eastern quartz core of the Lindvikskollen pegmatite. B – Tourmaline crystal cluster in the wall zone of the Lindvikskollen pegmatite. C – Wall of the West Mine of the Lindvikskollen pegmatite showing the quartz core on the left and the blocky intermediate zone on the right with a line of black tourmaline crystals (see white arrow). The width of the photograph is about 3 m. D – A cluster of fine-grained, granoblastic tourmalines in albitite close to the contact of the Lindvikskollen pegmatite. E – Enrichment of tourmaline in the Ramfoss pegmatite. Photograph by Øivind Thoresen. F – Rock slab showing a massive quartz from the Spro pegmatite cross-cut by a fine-grained albite vein containing black tourmaline. The slab is 25 cm in length.

interpreted as the pegmatite crystallization age (Müller et al., 2017). Rosing-Schow et al. (2023) confirmed the age with 1082.2 ± 4.8 Ma by using a different columbite-(Mn) crystal.

The *Dalane pegmatite* forms an approximately 50 m long and up to 6 m wide, E-W-striking lens hosted by granitic gneiss (De la Cruz, 2021). The pegmatite shows a distinct zoning with a granitic border zone up to 10 cm wide, a 1–3 m wide wall zone, and a meter-sized central quartz core. Major minerals in the medium- to coarse-grained border zone are K-feldspar, plagioclase, quartz, and biotite. In the wall zone, crystal sizes increase to half a meter and muscovite is very abundant whereas biotite

is less common. Black tourmaline is a minor mineral forming elongated prismatic crystals up to 50 cm in length. Tourmaline contains muscovite along the cleaveage planes, a characteristic feature of the Dalane tourmalines. Accessory minerals include garnet, beryl, fergusonite-(Y), zircon, monazite-(Ce), xenotime-(Y) and allanite-(Ce) (De la Cruz, 2021).

The *Havredal pegmatite* forms an E-W striking, dyke-like body which is approximately 100 m long and up to 15 m wide (Andersen, 1931; De la Cruz, 2021). The mineralogical-textural zoning is only weakly developed. Major minerals are K-feldspar, plagioclase, muscovite, and quartz. Black tourmaline is a common minor mineral, while biotite is rare. This pegmatite is characterized by the occurrence of hematite masses up to 20 cm, which were mined in the 17th century. The host rocks are migmatitic gneisses and metagabbros that underwent partial albitization before pegmatite intrusion. The albitization event was dated by Engvik et al. (2011) between 1090 and 1084 Ma based on U-Pb ages of metasomatic rutile.

The *Ramfoss pegmatite* is part of the Kongsberg-Modum pegmatite district in the *Kongsberg LU* (Fig. 1). The pegmatite forms a relatively small, 15 m long and 6 m wide, isolated body (De la Cruz, 2021). Major minerals include K-feldspar, plagioclase, albite, quartz, and muscovite. Similar to Havredal, black tourmaline is a common minor mineral (Fig. 3E). Accessory minerals are allanite-(Y) and titanite. Isochron Pb-Pb albite–titanite–turmaline–apatite dating of the Ramfoss pegmatite yielded a crystallization age of 1045 ± 12 Ma (Andersen and Grorud, 1998). The host rocks are quartzites of the Modum Complex (Viola et al., 2016) with a maximum sedimentation age of 1434 ± 29 Ma (Andersen and Grorud, 1998). Besides quartzites, the Modum complex comprises micaschists and feldspathic gneisses with minor occurrences of marbles and calcsilicate rocks (Jøsang, 1966; Munz, 1990). The entire sequence was intruded by gabbros at 1224 ± 15 Ma (Munz et al., 1994). Similar to the Kragerø area, the Modum gabbros and some metasediments underwent fluid-driven albitization prior to pegmatite emplacement at 1080 ± 3 Ma (Munz et al., 1994).

3.1. The Spro pegmatite belongs to the Østfold-Halland pegmatite district in the Idefjorden

LU (Fig. 1). The pegmatite forms a large, isolated body approximately 230 m long with variable thickness ranging from 0.5 to 25 m (Bugge, 1955; Faria, 2019). The subvertical pegmatite dyke intruded a regional, N-S-striking shear zone. The pegmatite consists of the major minerals quartz, muscovite, K-feldspar, and plagioclase (oligoclase) and accessory samarskite-(Y), euxenite-(Y), columbite-(Fe), thorite, and monazite-(Ce) (Raade, 1965; Faria, 2019). The pegmatite is zoned in texture and mineral abundance from the wall zone and inwards. Plagioclase is abundant in the wall zone and decreases towards the core, whereas muscovite abundance and crystal size increase away from the wall zone. A quartz core is not developed. In addition, irregular veins and masses of fine-grained saccharoidal albite, associated with black tourmaline, muscovite, fluorite, topaz, beryl, microlite group minerals, apatite, and calcite crosscut and replace coarser grained parts of the pegmatite (Fig. 3F). These veins are considered albite replacement zones or secondary units according to Jahns (1955). The pegmatite host rocks comprise granitic gneiss of the granitic to tonalitic suite of the Nesodden peninsula and metasedimentary amphibole gneisses with protolithic ages 1542 ± 5 Ma and 1900 to 1600 Ma, respectively (Skiöld, 1976; Jacobsen and Heier, 1978; Pedersen et al., 1978; Pózer Bue, 2008). These rocks were deformed under amphibolite-facies metamorphism between 1041 and 1033 Ma (Narum et al., 2021). The age of emplacement of the Spro pegmatite is 1036 ± 2 Ma based on U-Pb columbite dating (Rosing-Schow et al., 2023).

4. Methods and sampling

4.1. Sampling

The samples used in this study were collected from pegmatites during fieldwork and in some cases from the mineral collection of the Natural History Museum, University of Oslo. The complete list of samples with petrographic descriptions and information about sample locations are provided in the Supplementary Material SMTable 1. The investigated materials include whole rock samples (WR, n = 15) and tourmaline crystals (n = 25) from six pegmatites. Whole rock sampling focused on the Lindvikskollen and Spro pegmatites and their host rocks. Five lithologies were sampled for bulk rock analyses at Lindvikskollen: the pegmatite wall zone (12062014), metagabbro about 2 m away from the pegmatite contact (12062015), and tourmaline-bearing albitite 8 m from the pegmatite contact (12062016). Samples farther away from the pegmatite include two albitite samples (12062026, 12062027), as well as a tourmaline-bearing granite dyke (12062031) and amphibolite (12062029) (Fig. 2). The samples for bulk rock analysis from the Spro locality include three granitic gneisses (04061802, 05061801, 05061803), three amphibole-biotite gneisses (05061802, 0406180, 05061804), one bulk sample of the Spro pegmatite wall zone (16091806) and one sample of the albite replacement zone (690).

4.2. Whole rock analysis

The pegmatite bulk rock samples comprise 25 kg of each of the wall zones of Lindvikskollen and Spro pegmatites and one 10 kg sample of the albite zone of the Spro pegmatite. The wall zone samples, which have a coarse-grained granitic texture, are considered to be representative of the initial pegmatite melt composition at the time of emplacement (e.g. Müller et al., 2022). The pegmatite and host rock samples were first crushed. In the case of the large pegmatite samples, multiple batches of crushed material were homogenized manually in a large plastic bucket. After homogenization, the crushed material was split with a closed-bin riffle sample splitter and milled down to grain sizes < 200 μm. The rock powders were sent for whole rock analyses to Activation Laboratories in Vancouver, Canada (Actlabs, 2023) in the case of the Lindsvikollen samples and to Bureau Veritas in Vancouver, Canada (Bureau Veritas, 2023) in the case of the Spro samples. The analytical methods include X-ray fluorescence (XRF) on fused lithium tetraborate discs for major elements, ion selective electrode (ISE) method for fluorine concentration, and inductively coupled plasma mass spectrometry (ICP-MS) on sodium peroxide fused disks for 72 minor and trace elements. Because the discs were fused in a Zr crucible and Lu was used as internal standard by Actlabs, those elements could not be measured for the Lindsvikollen samples. The complete data set including limits of detection is provided in the Supplementary Material SMTable 2.

4.3. EPMA and backscattered electron imaging

The electron probe microanalysis (EPMA) was performed to determine the major and minor element concentrations of tourmaline. Tourmaline samples were prepared either as polished petrographic sections with a thickness of about 300 μm (for use of LA-ICP-MS as well) or as 1-inch epoxy mounts. Prior to EPMA the crystals were examined by backscattered electron SEM imaging to reveal intra-granular zoning and micro-inclusions. The instrument used was a CAMECA SX100 electron microprobe with 5 wavelength-dispersive spectrometers based at the Department of Geosciences of the University of Oslo. Analytical conditions were the following: accelerating voltage of 15 kV, beam current of 15nA, beam diameter between 1 and 3 μm, and counting time on peak of 10 s. The calibration standards used were synthetic compounds with characteristic X-ray lines in parentheses: Al_2O_3 (Al Kα), MgO (Mg Kα), Cr_2O_3 (Cr Kα) and Fe metal (Kα), and the minerals wollastonite for Si (Kα) and Ca (Kα), pyrophanite for Ti (Kα) and Mn (Kα), orthoclase for K

(Kα), albite for Na (Kα) and fluorite for F (Kα). Intensity data were corrected for both inter-element overlaps, and for matrix effects using the PAP procedure (Pouchou and Pichoir, 1984).

The contents of Li_2O, B_2O_3, and H_2O were approximated based on stoichiometry and neutral charge balance from EPMA data using an Excel spreadsheet developed by Ben Williamson of the University of Exeter, UK. The estimated contents were the basis for calculating site assignments and tourmaline mineral formulae. In this approach, B_2O_3 and H_2O were calculated assuming a fixed B concentration of 3 apfu and OH + F at 4 apfu. Li_2O contents were calculated after normalization to 15 total cations, where Li = 15-total (T + Z + Y). This is the recommended approach for tourmaline with low Li contents and minor B in the tetrahedral site (Henry et al., 2011). In some cases, the Li values calculated from EPMA data are not in agreement with measured values by LA-ICP-MS from the same sample. Because of this discrepancy, the Li concentrations presented in the text are those measured by LA-ICP-MS only. The complete EPMA data set is provided in the Supplementary Material SMTable 3.

4.4. LA-ICP-MS

The laser ablation inductively coupled plasma mass spectrometry (LA-ICP-MS) was applied to selected tourmaline samples for trace element analysis. The equipment used was the Bruker Aurora Elite quadrupole ICP-MS combined with a Cetac LSX-213 G2 + laser microprobe based at the Department of Geosciences, University of Oslo. The software utilized for data treatment was Glitter (Griffin, 2008). Each analytical cycle consisted of 3 spots on a synthetic glass reference sample (NIST SRM 610), 16 spots on the tourmaline crystals, and 2 spots on a basaltic glass standard sample (BCR-2G). The laser was operated with a spot size between 40 and 100 μm depending on the crystal size and laser frequency of 10 to 20 Hz. Determined trace element concentrations and the limits of detection (LOD) are provided in the Supplementary Material SMTable 4.

4.5. SIMS

Secondary ion mass spectrometry (SIMS) was used to analyse the B isotope ratios of selected tourmaline samples. The B isotope analyses were done on the same 1-inch, polished grain mounts used for EPMA and LA-ICP-MS analyses, after cleaning in an ultrasonic ethanol bath and then sputter-coated with a ~ 35 nm thick gold coating. SIMS analyses were performed, using a CAMECA IMF 1280-HR instrument at the GFZ German Research Centre for Geosciences in Potsdam, Germany. The SIMS operated with an acceleration voltage of 13 kV and $^{16}O^-$ primary beam current of 5nA which was focused to a spot ~ 5 μm diameter on the sample surface. Secondary ions were accelerated at nominal 10 kV with no voltage offset applied. Each analysis was preceded by a five-minute pre-sputter to remove the surface gold coating and establish stable sputtering conditions. Analyses were done in multi-collector mode with faraday cup detection, each analysis consisting of 20 ratio measurements. The mass resolving power (M/ΔM) of 2423 was more than enough to resolve interference of $^{10}B^1H$ on ^{11}B and of $^9Be^1H$ on ^{10}B. Tourmaline reference materials Harvard #108796 dravite, #112566 schorl, and #98144 elbaite (Leeman and Tonarini, 2001) were used to determine instrumental mass fractionation (IMF) and to assess analytical uncertainty. The precision of single analyses (1 SD/mean of 20 cycles) was typically 0.1 ‰. The repeatability (1SD/mean) of multiple analyses of a single reference tourmaline was 0.32 ‰ for schorl (n = 13), 0.31 ‰ for dravite (n = 12), and 0.6 ‰ for elbaite (n = 12). A slight chemical matrix effect is shown by differences in average IMF values: schorl = 0.976865, dravite = 0.975380, and elbaite = 0.973477 (all data are given in Supplementary Material SMTable 5). None of the tourmalines in this study are close to elbaite in composition so we used the average combined IMF factor of schorl and dravite reference tourmalines to correct the unknown samples. The combined repeatability for these reference materials (1SD/mean = 0.84 ‰, n = 25) is taken as an estimate of total analytical uncertainty. The IMF-corrected $^{11}B/^{10}B$ ratios were converted to $\delta^{11}B$ relative to NIST SRM 951 using the $^{11}B/^{10}B$ value of 4.04362 +/- 0.00137 (Catanzaro, 1970).

5. Results

5.1. Lithochemistry of pegmatites and host rocks at Lindvikskollen and Spro sites

5.1.1. Lindvikskollen

The wall zone of the Lindvikskollen pegmatite and the tourmaline-bearing granite dyke have granitic compositions according to the R1-R2 diagram of De la Roche et al. (1980) in Fig. 4A and they are both weakly peraluminous (Aluminum Saturation Index – ASI = 1.00 to 1.05 calcualted according to Frost and Frost, 2008). The dyke sample classifies as A-type granite and has much higher K_2O contents than the pegmatite which has I-type granite affinity (Fig. 4B; Supplementary Material SMTable 2). Both the metagabbro and amphibolite plot in the syeno-gabbro field of Fig. 4A. Albitites, which are products of Na metasomatism of the metagabbro (Engvik et al., 2011, 2014, 2018), are not plotted in Fig. 4A. The albitites have high Na_2O (8.6 to 10.1 wt%) and B contents (up to 2380 ppm). Other distinctive features of albitite are high TiO_2 (up to 4.8 wt%), high Sr and Ga, and low Fe_2O_3 (Supplementary Material SMTable 2).

The trace-element contents of the rock samples are plotted in Fig. 4C on an upper-continental-crust (UCC)-normalized multielement diagram. All samples from the Lindvikskollen area show overall similar distribution patterns characterized by depletions in Ba, Sr, and REE relative to the UCC composition, and enrichments in B. Characteristic features of the pegmatite wall zone, amphibole gneiss, and the tourmaline granite are higher Th, Nb and Ta contents than the metagabbro and the metasomatic albitite derived from it. The REE patterns of the Lindvikskollen rocks show some variability (Fig. 4D). The amphibole gneiss and granite dyke samples have relatively flat patterns and the strongest REE enrichment, excepting the negative Eu anomaly of the granite. The metagabbro and albitites are enriched in LREE relative to HREE and show weak positive or negative Eu anomalies, respectively. The pegmatite wall zone has lowest REE, a positive Eu anomaly, attributed to the high plagioclase content in the sample, and is slightly enriched in La and HREE.

5.1.2. Spro

The Spro granitic gneisses classify as A-type granites (Fig. 4A and B). The orthogneisses have variable granodioritic to granitic compositions with SiO_2 contents between 62 and 73 wt% and $Na_2O + K_2O$ values of approximately 6 wt%. Both the granitic and amphibole-biotite gneiss are peraluminous with ASI values of 1.08 and 1.58, respectively. The amphibole-biotite gneiss has a granitic I-type signature, whereas the granitic gneiss and the Spro pegmatite have marginal A-type granite affinity (Fig. 4B).

On the UCC-normalized multielement diagram the amphibole-biotite and granitic orthogneisses are slightly depleted in Sr and Ti and slightly enriched in Rb, Y, and Yb (Fig. 4E). Otherwise, the amphibole-biotite gneisses correspond roughly to the upper continental crust composition. Their most distinct features are relatively strong depletions in Ba, Sr and Ti and enrichments in Rb, Y, and Yb. The pegmatite samples show distinctly different patterns characterized by strong depletion in Ba, La, Ce, Sr, Nd, Sm, Zr, Hf and Ti, whereas Nb and Ta are enriched. The latter are mostly bound in columbite group minerals, a common accessory mineral of the Spro pegmatite. Among the two pegmatite samples, the albite replacement zone (sample 690) is more depleted in Sr while much more enriched in Nb, B and Ta. Compared to the relative similar patterns of pegmatite and host rocks at Lindvikskollen, the Spro pegmatite and host rocks have very different trace-element signatures. The REE distributions shown in Fig. 4F confirm this contrast: all gneisses have

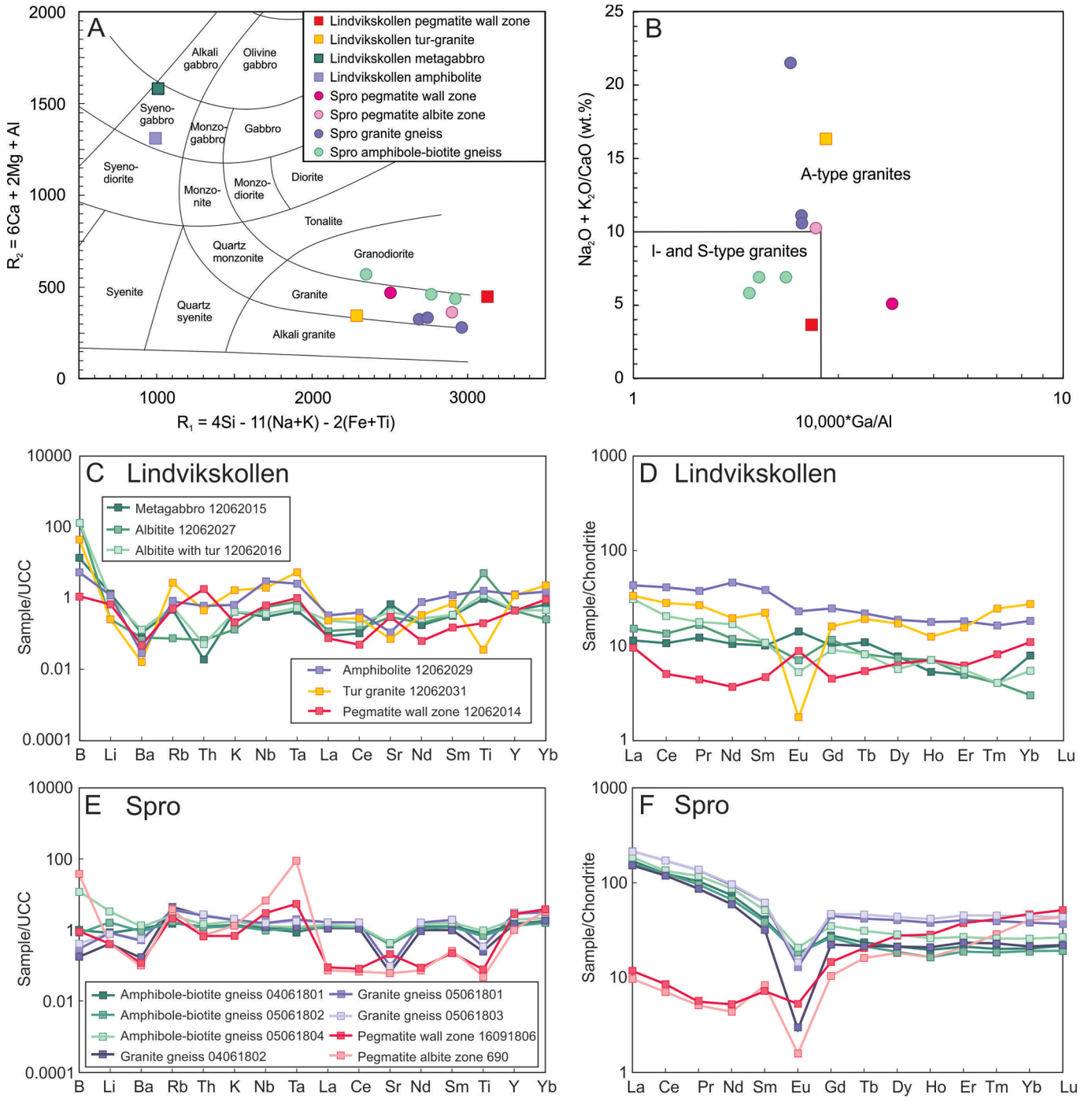

Fig. 4. A – R1-R2 classification diagram of De la Roche et al. (1980) with whole-rock data from the Lindvikskollen and Spro igneous rocks. B – Lindvikskollen and Spro data in the 10,000*Ga/A1 versus (K_2O + Na_2O)/CaO plots for discrimination of A- type and I-/S-/M–type granites according to Whalen et al. (1987). C to F – Upper-continental-crust-(UCC)-normalized multielement plots (A and C) and chondrite-normalized REE patterns (B and D) of Lindvikskollen and Spro pegmatites and host rocks. UCC values are from Rudnick and Gao (2003) and REE values from Anders and Grevesse (1989).

similar patterns characterized by strong LREE enrichment, and a flat HREE distribution. The negative Eu anomaly shows, however, some variations. By contrast, the pegmatite samples are depleted in LREE relative to HREE, and the latter shows a progressive enrichment towards Lu.

6. Tourmaline composition

6.1. *Variation of tourmaline chemistry among different pegmatites*

Prior to chemical analyses, the tourmalines were examined by SEM to reveal growth and alteration zoning as well as mineral inclusions. Tourmalines from the Lindvikskollen, Ramfoss, Havredal, and Spro pegmatites appear homogenous on backscattered electron images with rare mineral inclusions. Examples from Lindvikskollen and Havredal are shown in Fig. 5A and 5B. Tourmalines from the Tangen and Dalane

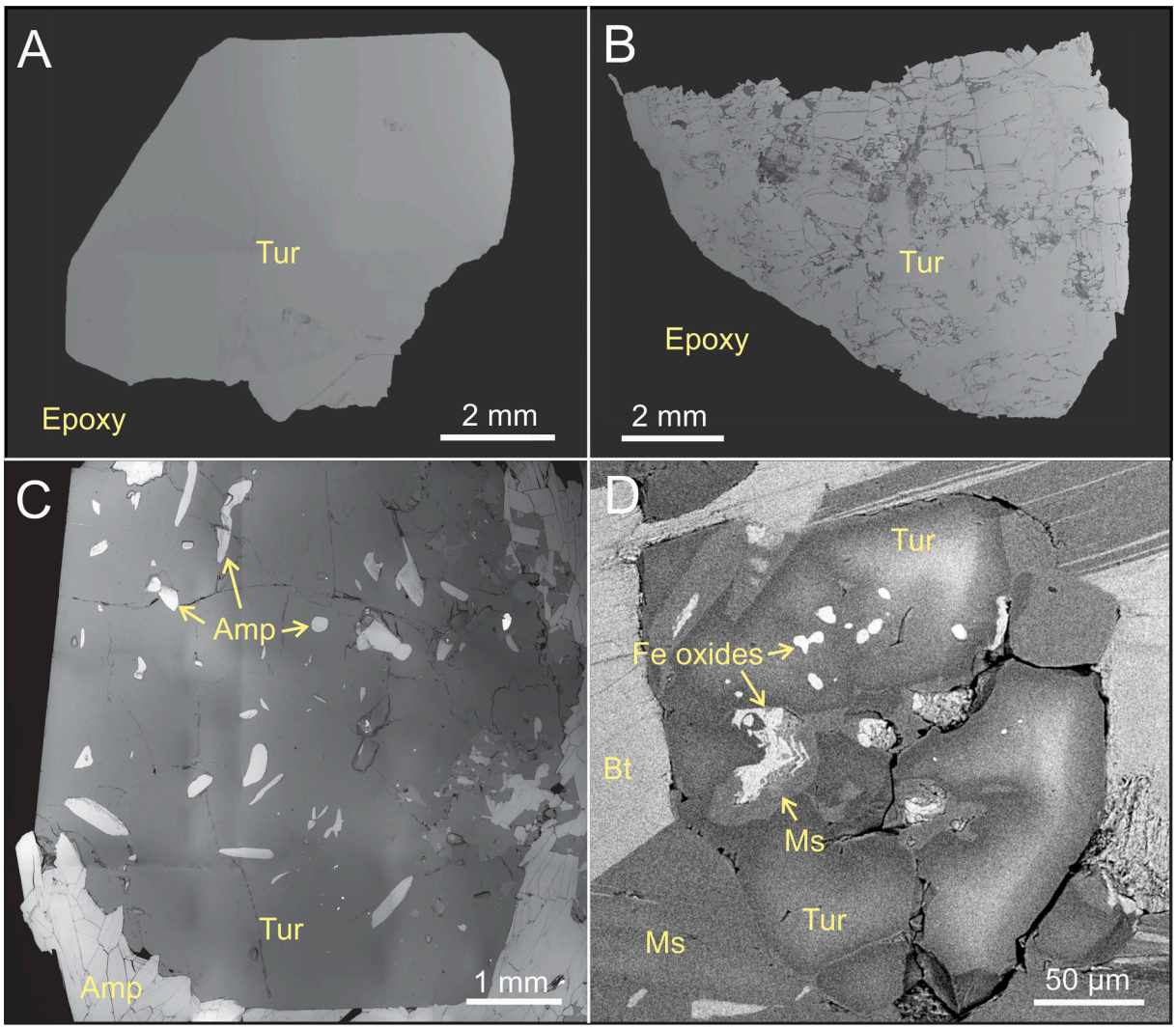

Fig. 5. Backscattered electron images of tourmalines. A – Fragment of euhedral tourmaline from the Lindvikskollen pegmatite (sample 20252), B – Fragment of euhedral tourmaline from the Havredal pegmatite (sample 20216), C – Tourmaline phenoblast in the metagabbro host rock at Lindvikskollen (sample 12062020) with abundant inclusions of amphibole. D – Tourmaline phenoblast in amphibole-biotite gneiss host rock at Spro (sample 05061804). Amp – amphibole, Bt – biotite, Ms – muscovite, Tur – tourmaline.

pegmatites are partially altered to mica and do not exhibit primary growth zoning. The much smaller tourmalines from the pegmatite host rocks of Lindvikskollen and Spro are rich in micro inclusions of mica, amphibole, quartz, feldspar, and Fe oxides and show features of granoblastic growth (Fig. 5C and D). The Spro host rock tourmalines are chemically zoned, as revealed by variable grey shades in the BSE image (Fig. 5D).

The tourmaline supergroup has a complex chemical composition with the generalized formula $XY_3Z_6(T_6O_{18})(BO_3)_3V_3W$ (e.g. Henry et al., 2011). The relative site abundance of cations and anions of the studied tourmalines are summarized in Table 2. All investigated tourmalines belong to the alkali-tourmaline group (Henry et al., 2011) based on the dominant occupancy of the X-site (Fig. 6A). The data show, however, a wide scatter across the alkali group field and a tendency for each pegmatite to plot distinct from the others. For example, the Tangen samples stand out with the highest alkali contents (Na = 0.94 apfu, K = 0.03 apfu), the Dalane tourmalines have the highest concentration of vacancies and the Lindvikskollen tourmalines plot along the Ca-Na + K join with very low X-site vacancy.

The variations in major element compositions are well illustrated in the ternary Fe-Al-Mg plot of Henry and Guidotti (1985) which also discriminates tourmaline of different geologic provenance (Fig. 6B). Tourmalines from the Spro, and Dalane pegmatites and from the Lindvikskollen granite dyke are Fe-rich and plot in field 2 “granitic pegmatites”. The Tangen tourmalines, which are richest in Fe, plot exclusively in field 3. All Lindvikskollen pegmatite tourmalines have low Al contents compared to the other tourmalines studied and form a group spanning fields 3 and 6 corresponding to “quartz-tourmaline rocks”. The Ramfoss tourmalines plot as a separate group in field 6 while tourmalines from the Havredal pegmatite and those from Spro and Lindvikskollen host rocks fall in fields 4 and 5 for “metapelites”. The “non-granitic” tourmaline chemistry of Lindvikskollen and Havredal pegmatites according to the provenance fields of Fig. 6B is indicative of the influence of hydrothermal processes.

The clustering of tourmaline from individual pegmatites and their host rocks is also clear in the Mg/(Mg + Fe) versus Xvac/(Xvac + Na) diagram (Fig. 6C). Tourmaline from the granite dyke and most of the pegmatite tourmalines, except Ramfoss and Havredal, plot in the schorlitic quadrant. Tourmalines from the metagabbro and albitite host rocks at Lindvikskollen, and from the amphibole-biotite gneiss at Spro plot in the dravite field with mg# {Mg/(Mg + Fe)} between 0.54 and 0.85. Interestingly, tourmalines in metagabbro and albitite have similar major element features, despite the very different bulk rock compositions. Tourmalines from the Spro and Tangen pegmatites are richest in

Table 2
Average results of tourmaline EPMA data (in wt.%). Standard deviation in parentheses.

Samples		Lindvikskollen			Tangen	Dalane	Havredal	Ramfoss	Spro	Host rocks			
		Wall zone	Inter. zone	Core zone						L. metagabbro	L. albitite	L. tourmaline granite	Spro gneiss
n	LOD	26	97	74	3	5	4	4	81	12	14	13	8
SiO_2	0.07	34.97 (0.37)	35.21 (0.30)	35.17 (0.29)	33.55 (0.18)	36.21 (0.20)	36.96 (0.35)	35.92 (0.15)	34.67 (0.31)	37.17 (0.14)	36.98 (0.24)	34.14 (0.21)	36.44 (0.40)
Al_2O_3	0.06	25.06 (0.61)	25.31 (1.16)	24.19 (0.59)	21.21 (0.29)	33.75 (0.19)	31.18 (0.29)	28.42 (0.11)	32.33 (0.55)	31.66 (0.27)	31.19 (0.61)	29.98 (0.66)	32.66 (1.31)
TiO_2	0.05	1.22 (0.21)	1.19 (0.36)	1.31 (0.14)	1.17 (0.03)	0.08 (0.03)	0.41 (0.04)	1.41 (0.07)	0.14 (0.11)	0.60 (0.04)	0.88 (0.31)	0.39 (0.03)	0.42 (0.15)
FeO	0.10	17.27 (1.22)	16.24 (1.23)	16.28 (0.87)	25.11 (0.28)	13.27 (0.19)	6.15 (0.11)	10.22 (0.15)	16.18 (0.59)	3.32 (0.19)	3.79 (0.49)	17.82 (0.67)	7.20 (1.34)
MgO	0.05	4.75 (0.99)	5.36 (0.79)	5.91 (0.72)	0.01 (0.01)	1.57 (0.03)	8.55 (0.10)	6.73 (0.14)	0.17 (0.15)	9.44 (0.1)	9.14 (0.30)	1.21 (0.09)	6.43 (0.18)
MnO	0.08	0.16 (0.03)	0.18 (0.06)	0.19 (0.04)	3.10 (0.05)	0.14 (0.02)	0.01 (0.02)	0.02 (0.01)	0.31 (0.09)	<0.08	0.01 (0.01)	0.95 (0.18)	0.02 (0.02)
Na_2O	0.05	2.21 (0.18)	2.15 (0.11)	1.98 (0.12)	2.66 (0.03)	1.66 (0.04)	2.26 (0.08)	2.02 (0.03)	2.37 (0.08)	2.50 (0.05)	2.62 (0.13)	2.40 (0.04)	1.91 (0.08)
$B_2O_{3\ calc}$		10.04	10.11	10.06	9.54	10.51	10.71	10.46	10.19	10.81	10.75	10.10	10.67
CaO	0.06	1.01 (0.36)	1.15 (0.24)	1.49 (0.26)	0.11 (0.03)	0.18 (0.05)	0.71 (0.04)	1.46 (0.11)	0.13 (0.04)	0.91 (0.07)	0.61 (0.26)	0.40 (0.11)	1.03 (0.32)
Li_2O_{calc}		0.23	0.24	0.29	0.84	0.30	0.20	0.52	0.22	0.45	0.52	0.06	0.30
H_2O_{calc}		3.38	3.36	3.36	3.25	3.58	3.68	3.58	3.08	3.61	3.62	3.47	3.60
K_2O	0.03	0.10 (0.02)	0.08 (0.02)	0.08 (0.01)	0.13 (0)	0.04 (0.01)	0.07 (0.01)	0.09 (0.01)	0.08 (0.01)	0.04 (0.01)	0.03 (0.01)	0.08 (0.03)	0.06 (0.01)
F	0.22	<0.22	0.27 (0.10)	0.24 (0.09)	<0.22	<0.22	<0.22	<0.22	0.93 (0.16)	0.26 (0.04)	<0.22	<0.22	<0.22
Total		100.49	100.75	100.43	100.75	101.35	100.92	100.88	100.41	100.67	100.23	101.01	100.84
Formula proportions based on 31 oxygen atoms (apfu)													
Si		6.06	6.05	6.08	6.11	5.99	6.00	5.97	5.91	5.98	5.98	5.88	5.93
Al		5.11	5.13	4.92	4.55	6.57	5.96	5.57	6.50	6.00	5.95	6.08	6.26
Ti		0.16	0.15	0.17	0.16	0.01	0.05	0.18	0.02	0.07	0.11	0.05	0.05
Fe^{2+}		2.50	2.34	2.35	3.83	1.84	0.83	1.42	2.31	0.45	0.51	2.57	0.98
Mg		1.22	1.37	1.52	0.00	0.39	2.07	1.67	0.04	2.26	2.20	0.31	1.56
Mn		0.02	0.03	0.03	0.48	0.02	0.00	0.00	0.04	0.00	0.00	0.14	0.00
Na		0.74	0.71	0.66	0.94	0.53	0.71	0.65	0.78	0.78	0.82	0.80	0.60
B		3.00	3.00	3.00	3.00	3.00	3.00	3.00	3.00	3.00	3.00	3.00	3.00
Ca		0.19	0.21	0.28	0.02	0.03	0.12	0.26	0.02	0.16	0.10	0.07	0.18
Li		0.16	0.17	0.20	0.62	0.20	0.13	0.35	0.15	0.29	0.34	0.04	0.19
OH		3.90	3.85	3.87	3.95	3.95	3.98	3.97	3.50	3.87	3.91	3.99	3.91
K		0.02	0.02	0.02	0.03	0.01	0.01	0.02	0.02	0.01	0.01	0.02	0.01
F		0.10	0.15	0.13	0.05	0.05	0.02	0.03	0.50	0.13	0.09	0.01	0.09
X Al		−0.62	−0.62	−0.77	−1.12	0.57	0.03	−0.23	0.43	0.07	0.07	0.03	0.27
X vac		0.05	0.06	0.04	0.01	0.43	0.15	0.07	0.18	0.06	0.07	0.11	0.20
Mg/(Mg + Fe)		0.33	0.37	0.39	0.01	0.17	0.71	0.54	0.02	0.83	0.81	0.11	0.61

LOD – limit of detection, Inter – intermediate, calc – calculated, L. – Lindvikskollen, n – number of analyses, X Al – Al apfu allocated to the X-site, Xvac – X site vacancy.
Structural formula based on 31 anions (O, OH, F). B_2O_3, H_2O and Li_2O calculated by stoichiometry for B = 3 apfu, OH + F = 4 apfu and Li = 15-total (T + Z + Y) and normalizing to 31 anions. See also explanation in section *Methods and Sampling*.0.36.

Fe with average Mg numbers of 0.02 and 0.01, respectively. The tourmalines from different zones of the Lindvikskollen pegmatite all have moderately high Fe, with an average Mg number of 0.36, but they overlap in a large field of Fig. 6C. Minor characteristics, which are not illustrated, are a strong F enrichment (0.9 wt%; 0.5 apfu) and low Ti (0.02 apfu) in the Spro pegmatite tourmalines and high Mn (0.48 apfu) in the Tangen tourmalines (Table 2).

Minor and trace elements of pegmatite tourmalines determined by LA-ICP-MS (Table 3) reflect predominantly the composition and fractionation degree of the pegmatite melt (e.g., Breaks et al., 2003; Beurlen et al., 2011; Zhou et al., 2021). Tourmaline of the most fractionated Tangen pegmatite, for example, is richest in incompatible elements such as Mn, Sn, Zn, Pb, and Ga (Fig. 7). The Spro tourmaline is outstandingly rich in Li contents. Tourmalines from more primitive pegmatites, such as Lindvikskollen, have elevated concentrations of compatible trace elements such as Sc and Ti. Tourmalines from pegmatite host rocks are richest in Ni and V.

The Lindvikskollen pegmatite is the only one from this study where tourmaline occurs in all mineralogical zones (Fig. 2B). The intra-pegmatite variability in tourmaline composition from the different zones is, however, minor (Tables 2 and 3, Figs. 6 and 7). The major elements show a minor increase of the Mg number, Mn, and Ca and a decrease of Na from the wall zone to the intermediate and core zone. Numerous trace elements show distinct trends (Fig. 7). For example, Sr, V, Ni, and Ca increase whereas K, Ga, Sn, and Sc decrease from the wall zone towards the core.

6.2. Boron isotopic compositions of tourmaline

The B isotope ratios were determined for tourmalines from the Kragerø pegmatites of the *Bamble LU* (i.e., Lindvikskollen, Tangen, Dalane, Havredal), the Ramfoss pegmatite of the *Kongsberg LU* and the Spro pegmatite of the *Idefjorden LU*. The $\delta^{11}B$ data are summarised in Table 4 (full data in Supplementary Material SMTable 5) and shown graphically in context with other regional studies (Fig. 8). The $\delta^{11}B$ values range overall from –13.5 ‰ to + 9.7 ‰ but it is important to note that the range for individual pegmatites is just 2 ‰ at most. The $\delta^{11}B$ values of tourmaline from all Kragerø pegmatites are similar. The Lindvikskollen and Tangen samples, from pegmatites 1300 m from each other, have indistinguishable values taking the uncertainty of about 1

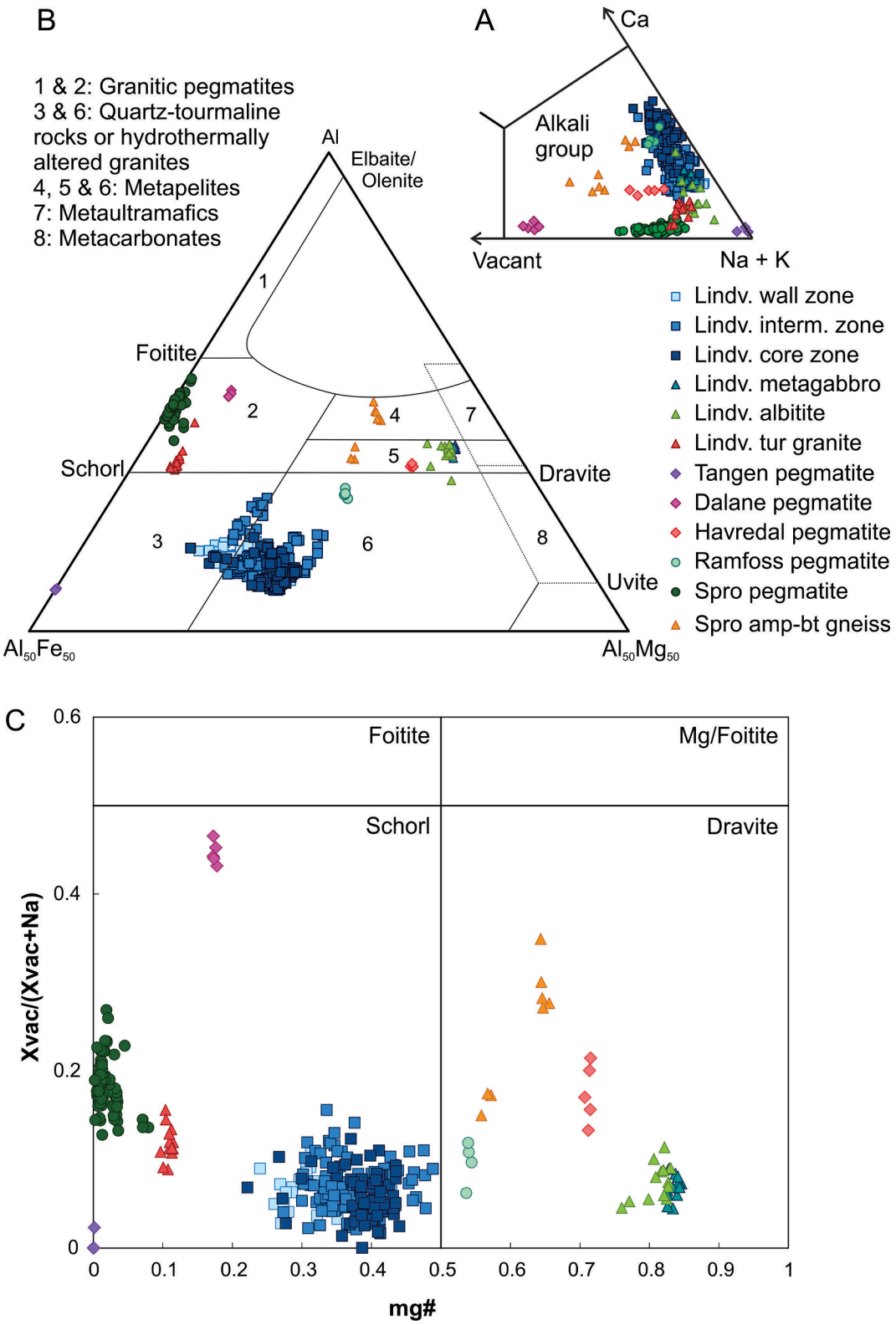

Fig. 6. A – Tourmaline classification according to Henry et al. (2011) using the occupancy of the X-site. B – Ternary Al50Fe50-Al-Al50Mg50 plot according to Henry and Guidotti (1985). Lindv.: Lindvikskollen; interm. zone: intermediate zone of the pegmatite; tur-granite: tourmaline-bearing dyke granite. C – mg# vs Xvac/(Xvac + Na) classification according to Henry et al. (2011).

permil into account. The Lindvikskollen tourmaline has $\delta^{11}B$ values from −1.9 to −1.0 ‰, averaging −1.4 ‰, while the Tangen $\delta^{11}B$ range is from –1.4 to −1.0 ‰, with an average of −1.3 ‰. Published $\delta^{11}B$ values determined by Bast et al. (2014) for tourmaline from the Lindvikskollen pegmatite (sample Li-8: −0.4 to + 3.6 ‰ $\delta^{11}B$) are in good agreement with our results but they are more variable and range to slightly higher values (Fig. 8). The borosilicate hellandite-(Y) is present in Lindvikskollen and it contains boron in tetrahedral coordination in contrast

Table 3
Average trace element concentrations of tourmalines (in ppm) determined by LA-ICP-MS, standard deviation in parentheses. Some average values for K, Ca, Ti and Mn have high standard deviations due to by contamination by microinclusions (see also Supplementary Material SMTable 4).

		Lindvikskollen pegmatite				Tangen pegmatite	Dalane pegmatite	Havredal pegmatite	Ramfoss pegmatite	Spro pegmatite	Host rocks			
		Wall zone	Intermediate zone	Core zone (West mine)	Core zone (East mine)						Lind. metagabbro	Lind. albitite	Lind. tourm.-granite	Spro gneiss
	LOD	n = 9	n = 8	n = 8	n = 8	n = 8	n = 8	n = 8	n = 8	n = 23	n = 8	n = 8	n = 4	n = 8
Li	0.5	23 (2)	50 (41)	15 (2)	13 (1)	50 (55)	56 (4)	2 (0)	6 (0)	400 (285)	3 (1)	6 (1)	130 (19)	16 (2)
Be	0.1	3 (1)	10 (12)	3 (2)	1 (0)	4 (1)	2 (0)	0 (0)	1 (0)	9 (2)	1 (0)	2 (3)	7 (1)	1 (0)
P	5	24 (8)	46 (39)	41 (51)	21 (1)	32 (3)	22 (3)	38 (4)	27 (3)	22 (2)	32 (4)	35 (8)	52 (30)	46 (15)
K	20	809 (36)	805 (124)	697 (25)	535 (8)	2618 (3539)	450 (3)	551 (37)	648 (25)	916 (666)	243 (43)	160 (53)	1496 (685)	344 (29)
Ca	85	7956 (481)	8517 (383)	12,784 (642)	12,424 (355)	1399 (463)	3248 (270)	4170 (361)	12,879 (2506)	1534 (1663)	6168 (741)	4409 (1659)	5757 (475)	7067 (2820)
Sc	0.3	374 (159)	267 (56)	111 (20)	71 (4)	13 (2)	61 (5)	42 (3)	67 (3)	1 (1)	39 (1)	27 (2)	178 (12)	30 (21)
Ti	9	9548 (356)	7087 (2265)	8904 (381)	7039 (177)	7130 (2813)	1233 (15)	2063 (47)	7213 (209)	1197 (1146)	3606 (244)	4179 (1186)	2363 (151)	3603 (3290)
V	0.8	68 (7)	143 (58)	288 (11)	210 (5)	8 (1)	6 (1)	199 (6)	135 (11)	13 (21)	1092 (34)	773 (146)	20 (7)	235 (69)
Cr	2	10 (1)	24 (4)	14 (2)	12 (1)	20 (2)	11 (2)	78 (13)	58 (16)	14 (10)	643 (131)	260 (114)	7 (0)	150 (29)
Mn	5	1292 (41)	1717 (260)	1284 (83)	1273 (16)	13,811 (3451)	1489 (24)	28 (3)	158 (11)	2467 (542)	39 (4)	44 5)	5829 (434)	427 (309)
Co	0.1	32 (2)	34 (5)	35 (0)	35 (1)	4 (5)	1 (0)	11 (0)	31 (1)	35 (13)	15 (1)	21 (4)	4 (2)	23 (3)
Ni	5	<5	11 (5)	43 (6)	12 (1)	5 (0)	<5	41 (4)	51 (3)	18 (23)	316 (12)	336 (27)	8 (0)	161 (185)
Cu	0.2	4 (0)	12 (15)	4 (0)	4 (0)	10 (11)	4 (0)	4 (0)	4 (1)	5 (1)	4 (0)	5 (1)	20 (5)	118 (288)
Zn	1	105 (7)	154 (20)	115 (6)	110 (1)	1586 (307)	826 (22)	8 (0)	14 (1)	831 (244)	11 (2)	11 (2)	343 (21)	180 (11)
Ga	0.1	134 (5)	114 (6)	88 (2)	70 (1)	292 (40)	130 (2)	69 (2)	57 (2)	91 (17)	46 (1)	47 (1)	84 (6)	33 (3)
Rb	0.1	<0.1	3 (6)	<0.1	<0.1	15 (34)	<0.1	<0.1	<0.1	6 (12)	1 (0)	<0.1	8 (6)	2 (2)
Sr	0.1	9 (1)	24 (6)	54 (2)	37 (1)	11 (6)	2 (0)	19 (3)	64 (41)	17 (11)	39 (5)	66 (19)	3 (1)	225 (145)
Y	0.1	10 (28)	204 (495)	103 (238)	<0.1	3 (4)	<0.1	<0.1	43 (121)	2 (2)	1 (0)	1 (1)	4 (3)	14 (22)
Zr	1	2 (2)	2 (2)	73 (88)	<1	<1	<1	<1	2 (4)	62 (73)	2 (0)	2 (0)	2 (0)	44 (49)
Nb	0.1	5.4 (4.6)	120.0 (222.0)	3.7 (4.9)	0.7 (0.1)	6.4 (12.5)	2.4 (0.1)	0.1 (0)	0.3 (0.1)	1.8 (1.7)	<0.1	<0.1	8.7 (1.0)	5.7 (15.5)
Mo	0.1	<0.1	0.2 (0)	<0.1	<0.1	0.1 (0)	<0.1	0.1 (0)	<0.1	<0.1	0.3 (0.1)	0.2 (0.1)	<0.1	0.3 (0.1)
Sn	0.1	74.3 (21.7)	43.9 (4.5)	32.3 (3.6)	13.6 (0.3)	153.3 (51.0)	12.2 (0.4)	4.7 (0.3)	3.2 (0.2)	3.3 (1.1)	2.7 (0.2)	2.0 (1.0)	59.3 (1.9)	2.9 (2.4)
Sb	0.1	<0.1	0.4 (0.7)	0.1 (0.1)	<0.1	0.3 (0.2)	0.1 (0.2)	0.1 (0)	<0.1	0.2 (0.1)	0.1 (0)	<0.1	0.1 (0.1)	0.8 (1.5)
Cs	0.1	<0.1	2.2 (5.1)	<0.1	<0.1	0.3 (0.3)	<0.1	<0.1	<0.03	1.0 (2.5)	<0.1	<0.1	2.5 (3.0)	0.9 (1.0)
Ba	0.1	<0.1	2.5 (3.4)	0.6 (0.2)	0.2 (0)	7.7 (12.6)	<0.1	0.7 (0.2)	0.5 (0.2)	1.0 (2.4)	0.3 (0.1)	0.3 (0.1)	3.5 (1.6)	0.6 (0.7)
La	0.01	9.97 (1.74)	4.95 (3.95)	4.28 (1.98)	2.25 (0.06)	2.58 (0.84)	3.33 (0.05)	1.71 (0.32)	5.39 (0.70)	1.68 (1.04)	3.90 (0.59)	2.88 (2.09)	12.29 (1.43)	2.55 (1.16)
Ce	0.03	17.41 (3.07)	8.34 (7.22)	8.28 (7.86)	3.12 (0.14)	2.38 (0.85)	6.29 (022)	3.57 (0.71)	196.31 (530.16)	2.76 (1.74)	7.85 (1.85)	5.16 (4.27)	26.76 (3.68)	4.88 (3.19)
Pr	0.01	1.93 (0.35)	1.10 (1.18)	1.27 (2.03)	0.24 (0.01)	0.10 (0.06)	0.63 (0.01)	0.33 (0.05)	21.35 (57.88)	0.28 (0.17)	0.78 (0.16)	0.54 (0.48)	3.04 (0.46)	0.68 (0.70)
Nd	0.04	6.28 (1.29)	5.61 (8.18)	5.15 (9.54)	0.63 (0.02)	0.22 (0.27)	1.69 (0.03)	0.98 (0.14)	77.26 (211.04)	0.78 (0.49)	2.48 (0.57)	1.84 (1.75)	9.23 (1.44)	2.57 (3.17)
Sm	0.02	1.24 (0.69)	8.27 (16.54)	3.44 (7.67)	0.09 (0.01)	0.06 (0.06)	0.45 (0.01)	0.15 (0.02)	16.75 (46.29)	0.17 (0.10)	0.31 (0.06)	0.25 (0.23)	2.33 (0.43)	0.61 (1.08)
Eu	0.01	0.19 (0.06)	1.25 (2.33)	0.65 (0.92)	0.29 (0.01)	0.02 (0.03)	<0.01	0.05 (0.01)	2.92 (7.07)	0.07 (0.05)	0.11 (0.01)	0.12 (0.04)	0.07 (0.03)	0.55 (0.22)
Lu	0.01	0.39 (0.87)	6.20 (14.62)	2.13 (4.65)	0.04 (0.01)	0.64 (0.94)	<0.01	<0.01	0.36 (0.94)	0.09 (0.12)	0.01 (0)	0.02 (0.02)	0.15 (0.10)	0.65 (0.76)

(*continued on next page*)

Table 3 (*continued*)

		Lindvikskollen pegmatite				Tangen pegmatite	Dalane pegmatite	Havredal pegmatite	Ramfoss pegmatite	Spro pegmatite	Host rocks			
Ta	0.04	1.81 (0.91)	5.31 (9.19)	0.42 (0.10)	0.07 (0.04)	1.19 (0.57)	0.26 (0.03)	0.12 (0.09)	0.09 (0.01)	2.28 (1.59)	0.60 (0.18)	0.18 (0.17)	2.04 (0.27)	0.75 (1.30)
W	0.02	<0.02	0.89 (1.58)	0.16 (0.42)	<0.02	0.31 (0.64)	0.03 (0.05)	<0.02	<0.02	0.25 (0.62)	0.04 (0.01)	0.05 (0.01)	<0.02	0.44 (1.08)
Pb	0.01	3.18 (1.84)	3.68 (1.84)	4.19 (2.40)	2.17 (0.04)	17.41 (8.88)	4.78 (0.10)	0.16 (0.02)	0.87 (1.59)	8.15 (5.09)	0.11 (0.13)	0.04 (0.01)	1.88 (0.38)	6.36 (1.67)
Th	0.01	0.16 (0.59)	1.06 (1.93)	8.20 (9.51)	<0.01	0.03 (0.03)	<0.01	<0.01	3.73 (11.00)	0.14 (0.29)	0.01 (0)	0.02 (0.02)	0.14 (0.07)	0.16 (0.15
U	0.01	6.0 (17.4)	109.0 (267.7)	24.7 (62.3)	<0.01	3.6 (9.4)	<0.01	<0.01	1.2 (3.8)	0.6 (1.0)	<0.01	0.1 (0)	1.4 (1.2)	0.7 (1.0)

LOD – Limit of detection. n – number of analyses.

to tourmaline. However, the extreme rarity of hellandite-(Y) compared to abundant tourmaline means that isotope fractionation between the two minerals has negligible effect on the tourmaline $\delta^{11}B$ values. The other tourmalines from the Kragerø field have slightly positive $\delta^{11}B$ values varying from + 0.6 to + 1.0, average + 0.8 ‰ (Dalane) and from + 1.8 to 2.4, average + 2.1 ‰ (Havredal). Thus, the total range of tourmaline B-isotope ratios from the Kragerø field in the *Bamble LU* including data from Bast et al. (2014) is −0.9 to + 3.6 ‰ $\delta^{11}B$.

Tourmaline of pegmatites in other Sveconorwegian lithotectonic units have very different $\delta^{11}B$ values than the Bamble occurrences. The tourmaline of the Ramfoss pegmatite (*Kongsberg LU*) has much higher $\delta^{11}B$ values, from + 9.5 to + 9.9 ‰ with an average of + 9.7 ‰, whereas the Spro tourmaline yielded strongly negative $\delta^{11}B$ values from −13.8 ‰ to −12.5 ‰, averaging −13.0 ‰. The B-isotopic composition of Spro pegmatite-hosted tourmaline agree with those from the host rocks: −14.8 ‰ to −12.9, average −13.5 ‰ $\delta^{11}B$ (Table 4).

7. Discussion

7.1. Tourmaline composition and implications for pegmatite melt fractionation

The investigated tourmalines from Sveconorwegian pegmatites plot predominantly in the schorl field, with some dravitic composition (Fig. 6C). They differ mainly in the mg# ratio and in trace and minor element concentration (Figs. 6 and 7). These differences can have four general causes: (1) the pegmatite melt source, (2) the degree and nature of melt fractionation, (3) fluid exsolution during pegmatite crystallization, and (4) interaction of the pegmatite melt with host rocks or external fluids.

The Lindvikskollen pegmatite tourmalines have higher Ca and Ti content than the other tourmalines (Fig. 6A and 7E), as well as elevated contents of Sc, V, Sr, Co, Zr, W, REE, U, and Th (Table 3). The relative enrichment of the compatible elements Ca, Ti, Sc, V, Co and Sr suggests that the Lindvikskollen pegmatite melt was rather primitive and little fractionated compared to the others. The wall zone whole-rock sample of the Lindvikskollen pegmatite shows a weak positive Eu anomaly (Fig. 4D), pegmatite K-feldspar has low Rb/Sr and extremely high K/Rb ratios (0.03 to 6 and 100 to 8000, respectively), and the pegmatite dark mica is Mg-rich (magnesian siderophyllite), all features indicating a low fractionation degree of the pegmatite melt (De la Cruz et al., 2021). Utilizing the tourmaline chemistry, the degree of fractionation can be illustrated by the Li + Mn versus Mg + Ti + Ca diagram according to Breaks et al. (2003). In this diagram, increasing Li + Mn or decreasing Mg + Ti + Ca corresponds to increasing fractionation of the pegmatite melt (Fig. 9). The Lindvikskollen tourmaline has low Li + Mn (<0.4 apfu). Tourmalines from the Dalane, Havredal, Ramfoss and Spro pegmatites have similar low Li + Mn values, and the low degree of fractionation of these pegmatites is reflected by their bulk chemistry and mineralogy. By contrast, the Tangen tourmaline has the highest concentrations of Fe and Na and is enriched in several incompatible elements including Mn, Li, Ga, Ba, and Rb (Table 3). Although the Tangen pegmatite intrudes the same metagabbro as the Lindvikskollen pegmatite, the two pegmatites being 1.3 km apart, their tourmalines are chemically distinct. On the Li + Mn versus Mg + Ti + Ca diagram, the Tangen tourmalines classify as tourmalines crystallized from a highly fractionated melt (Fig. 9). Also, the major feldspar of the Tangen pegmatite is albite (variety cleavelandite) rather than the calcic plagioclase of the more primitive Lindvikskollen pegmatite. Green (1956) suggested that the Tangen pegmatite represents a fractionated melt derived from the nearby, much larger Lindvikskollen pegmatite, both pegmatites being situated on the same NW to WNW striking structure. The difference in tourmaline composition in the two pegmatites is consistent with this hypothesis.

At Lindvikskollen, tourmalines occur in all zones of the pegmatite as well as in the metagabbro and albitite host rocks close to the pegmatite

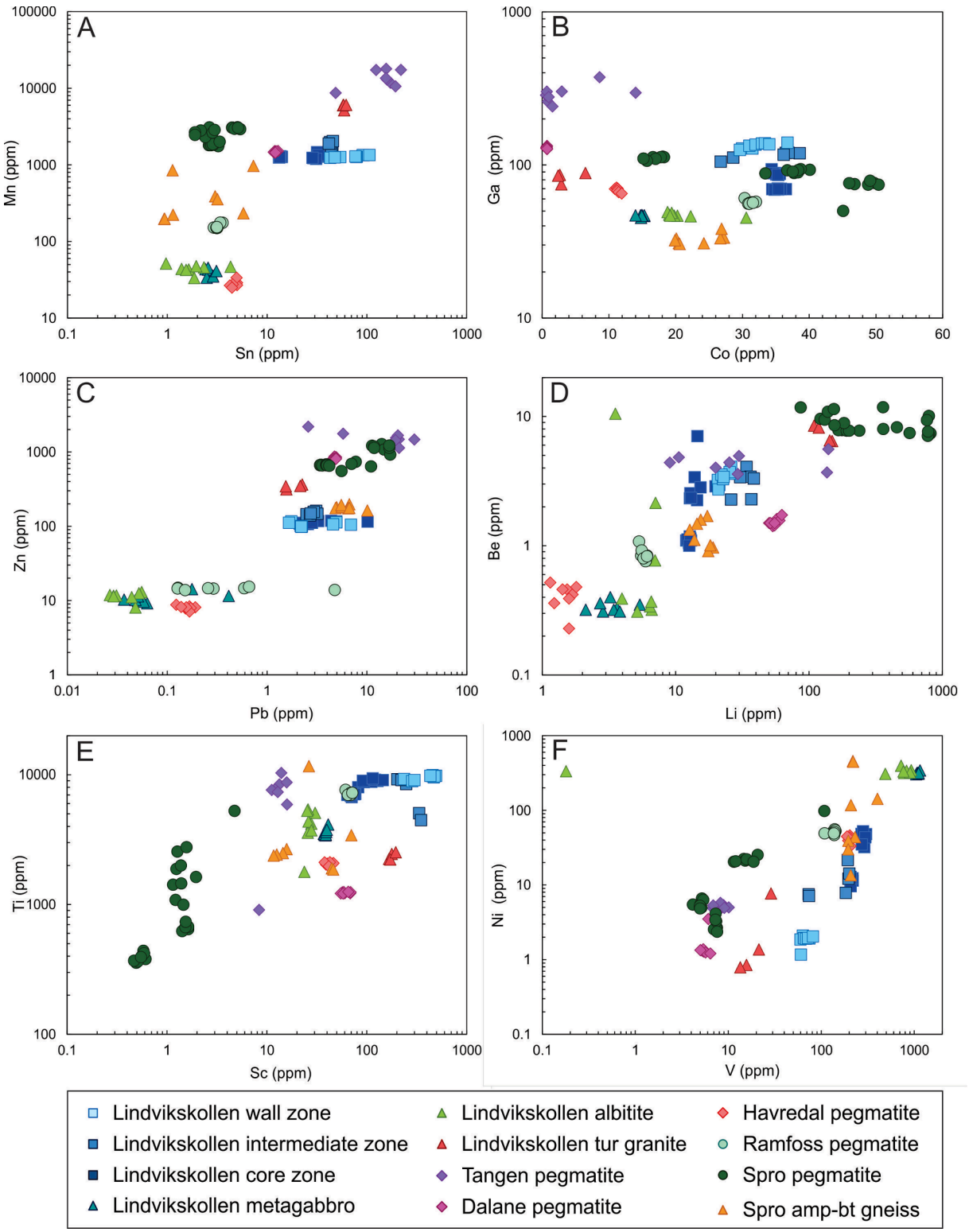

Fig. 7. Selected trace element plots of tourmaline from the investigated pegmatites and their host rocks.

contact (<10 m) (Fig. 2B). The element chemistry of all pegmatite-hosted tourmalines is relatively similar with only minor variations from the wall zone, intermediate zone and core zone, as well as between the two major core zones (East and West mine). Magnesium numbers vary from 0.33 to 0.39 (Table 2), implying that the Lindvikskollen pegmatite melt was rich enough in Fe and Mg to crystallize schorl throughout the entire sequence of wall, intermediate, and core zones (Fig. 2B). Thus, considering the similarity in tourmaline composition, the pegmatite melt underwent only minor internal fractionation (see also Fig. 9A).

The granoblastic textures of tourmaline (Fig. 5C), the location of host rock tourmaline at Lindvikskollen and Spro close to the pegmatite contact (<10 m), and the elevated B contents of > 200 ppm of host rocks (samples 12,062,015 and 05061804) near the contact suggest that the

Table 4
Statistical summary of B isotopic composition of tourmaline samples given as $\delta^{11}B$ values (in permil relative to NBS SRM-951 standard).

Locality	Litho-tectonic unit	Sample nr.	Origin of samples	$\delta^{11}B_{low}$	$\delta^{11}B_{high}$	$\delta^{11}B_{mean}$	SD	n
Lindviks-kollen	Bamble	20,252	Pegmatite core	−1.9	−1.0	−1.4	0.3	5
Tangen	Bamble	20,241	Pegmatite core	−1.4	−1.0	−1.3	0.2	9
Dalane	Bamble	13,051,920	Pegmatite intermediate zone	0.6	1.0	0.8	0.1	7
Havredal	Bamble	20,216	Pegmatite intermediate zone	1.8	2.4	2.1	0.2	5
Ramfoss	Kongsberg	20,091	Pegmatite intermediate zone	9.5	9.9	9.7	0.1	6
Spro	Idefjorden	690a, 690b, 690c	Albite replacement zone in pegmatite core	−13.8	−12.5	−13.0	0.1	41
Spro	Idefjorden	05,061,804	Amphibole gneiss 8 m from pegmatite contact	−14.8	−12.9	−13.5	0.6	8

SD – standard deviation in permil; n – number of analyses.

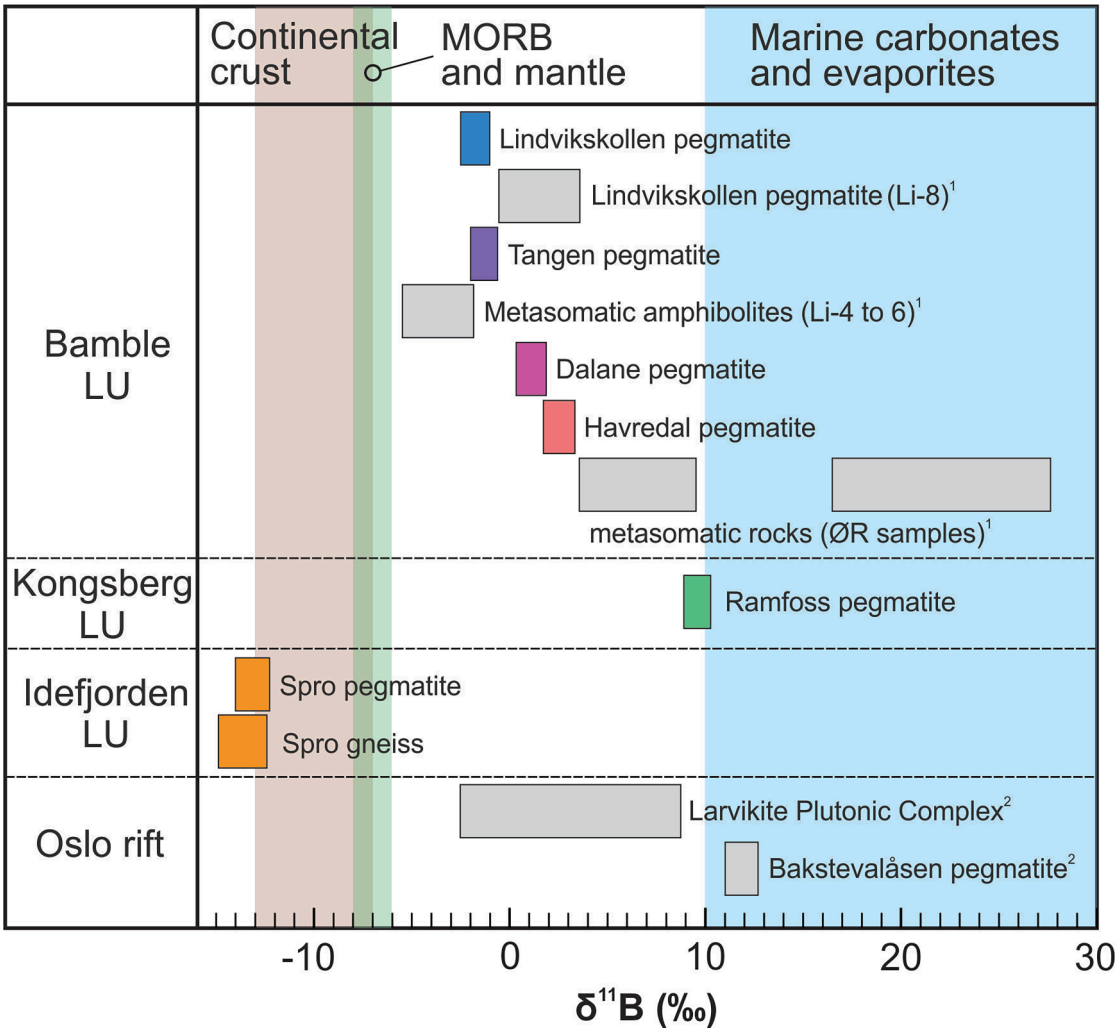

Fig. 8. δ11B value ranges of analysed tourmalines (colored squares) compared to the composition of different B source reservoirs (continental crust and marine evaporates: Van Hinsberg et al., (2011a); MORB and mantle: Marschall, 2018) and to published $\delta^{11}B$ data from the Sveconorwegian Bamble LU and the Permian Oslo rift (grey squares): [1] Bast et al. (2014) and [2] Sunde et al. (2020), respectively. LU- Lithotectonic unit.

host rock dravitic tourmaline formed by infiltration of aqueous, B-bearing fluids derived from the crystallizing pegmatite. This is supported by the fact that host rock tourmalines commonly replaced biotite and hornblende and inherited some of their chemical characteristics, as reflected by high Ni, V, and Cr, for example (Fig. 7F; Table 3). The Lindvikskollen host rock tourmalines also incorporated Na from the Na-metasomatised gabbro and albitite (Fig. 9B). In the Spro area, the host rock tourmalines have less Na than those in the pegmatite (Fig. 9C), because the host rocks are low in Na (Supplementary Material SMTable 2).

7.2. Genetic implications of the boron isotopic signature of tourmalines

The B-isotope values of tourmaline from the Sveconorwegian pegmatites show a high variability overall. However, the value ranges for samples from individual lithologic units (Bamble, Kongsberg and Idefjorden) are relative narrow and regionally distinct (Fig. 8). Importantly, only the pegmatite at Spro has tourmaline with a negative B-isotopic signature typical for the continental crust and S-type granites (−13.8 to −12.5 ‰) and in good agreement with the host rock gneiss (−14.8 to −12.9 ‰). Tourmalines from all other pegmatites in this study have much heavier isotope signatures (−1.9 to + 9.9 ‰) than either the continental crust or unaltered MORB and the upper mantle.

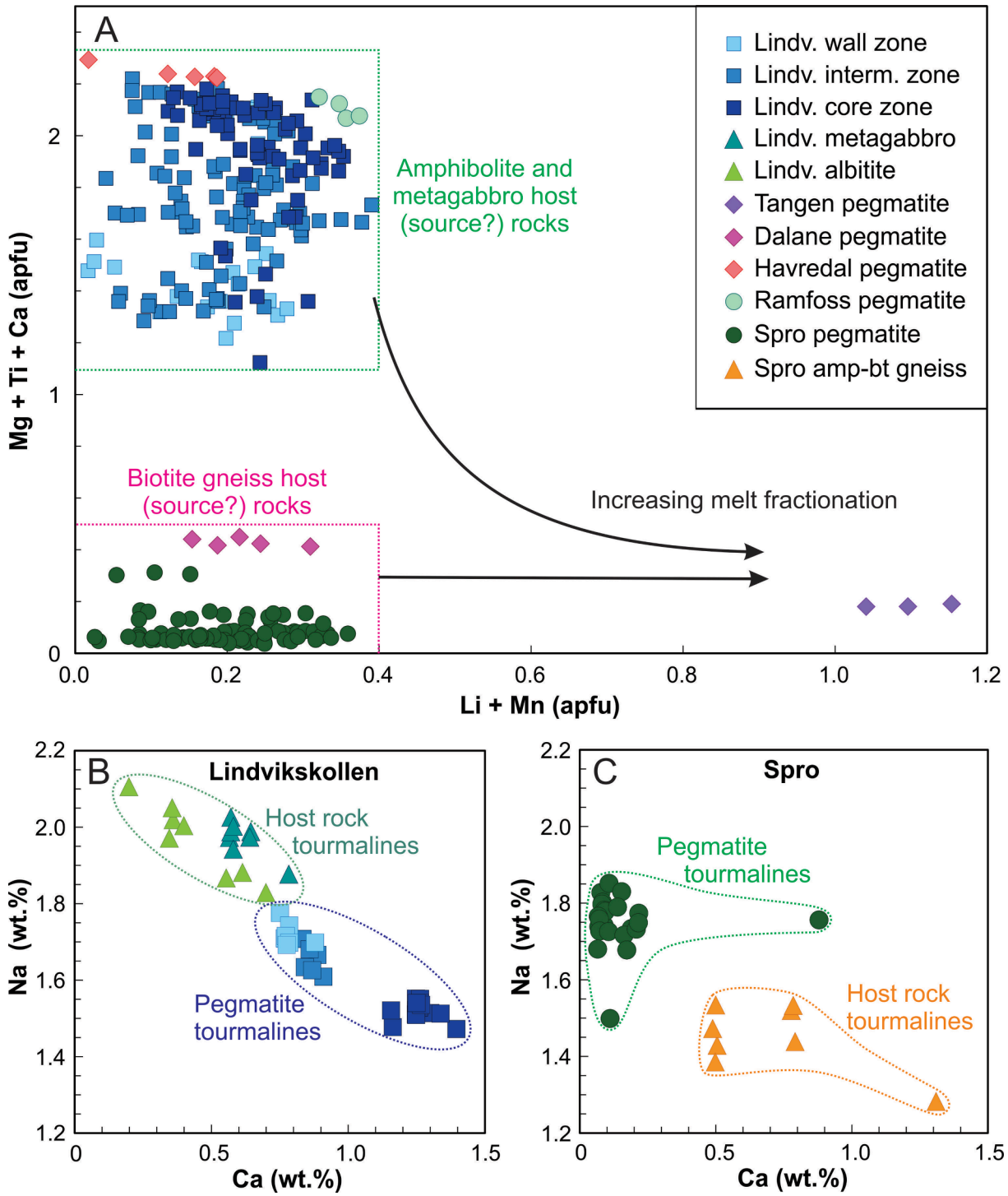

Fig. 9. A – Total Li + Mn vs Mg + Ti + Ca (apfu) diagram for tourmaline compositions by Breaks et al. (2003). According to Breaks et al. (2003), increasing Li + Mn in magmatic tourmaline corresponds to increasing fractionating degree of the host melt. The boxes for amphibole-biotite gneiss and amphibolite/metagabbro identify the host rocks of the pegmatites from this study. Composition of tourmaline from the host rocks are not shown in A. B – Na versus Ca plot of Lindvikskollen tourmalines from the pegmatite and its host rocks. C – Na versus Ca plot of Spro tourmalines from the pegmatite and its host rock.

Fundamentally, two processes can result in isotopically heavy B in a pegmatite melt: (1) secondary influx of external, heavy B from the host rocks during melt transport and/or crystallization, or (2) primary uptake of isotopically heavy B in the melt source. Before discussing these it is important to recall that magmatic processes of partial melting or fractional crystallization have very little effect on the B isotope composition of tourmaline because of the high temperatures involved (Marschall and Jiang, 2011; Trumbull and Slack, 2018; Cheng et al., 2022).

Process (1), assimilation of heavy B from the host rocks during melt transport or emplacement, is inconsistent with the narrow $\delta^{11}B$ range of tourmalines from the Kragerø pegmatite field regardless of variable local host lithology and of the location of the tourmaline within single zoned pegmatites (in the case of Lindvikskollen).

Therefore, process (2), primary uptake of isotopically heavy B from the melt source, is the better explanation for the narrow range of $\delta^{11}B$ values in the Kragerø pegmatites from the *Bamble LU* (−1.9 to + 2.4 ‰

$\delta^{11}B$) and for the heavier values for tourmaline from the Ramfoss pegmatite in the *Kongsberg LU* (+9.5 to + 9.9 $\delta^{11}B$). The Ramfoss values plot close to the fields of marine evaporates and carbonates on Fig. 8. The Ramfoss pegmatite occurs in quartzites of the supracrustal sequence of the Modum Complex, which contains intercalations of marbles and calcsilicate rocks. For the Kragerø pegmatites and Lindvikskollen, there is support for an isotopically heavy source from the work of Bast et al. (2014), who reported heavy B-isotope signature of tourmaline from metasomatised country rocks (Fig. 8). The authors cited evidence for regionally widespread Na-metasomatism in the Kragerø and Modum areas of the *Bamble LU* during a late stage of the Sveconorwegian orogeny, between 1110 and 1070 Ma, that involved hydration and enrichment in Na, Cl, B and P (Engvik et al., 2011, 2014, 2018). They hypothesized that these fluids, carrying isotopically heavy B, were most likely sourced from metamorphosed, Mesoproterozoic shallow marine sediments which are common in the *Bamble and Kongsberg LUs*, such as the Coastal Quartzite Complex in the Kragerø area (e.g. Nijland et al., 2014) and in the Modum Complex hosting the Ramfoss pegmatite (Munz et al., 1994). We suggest that during Na-metasomatism, these fluids imprinted their heavy B isotopic signature to the affected rocks of the *Bamble and Kongsberg LUs*, from which the pegmatite melts were later derived.

Sunde et al. (2020) also reported heavy B isotope signatures in tourmalines from alkaline pegmatites of the Permian Larvik Plutonic Complex in the Oslo rift (Fig. 1). Most of the alkaline pegmatites studied occur about 30 km NE of the Kragerø pegmatite field. The B isotope compositions of the Larvik tourmalines are in the same range as the Sveconorwegian *Bamble and Kongsberg LUs* tourmalines reported here (Fig. 8). Sunde et al. (2020) argued that the heavy isotopic signature of tourmaline in the alkaline pegmatites was caused by external B from fluids derived from contact metamorphism of marine Ordovician-Silurian sediments surrounding the Larvik Plutonic Complex. These sediments were derived from erosion of the nearby and underlying crystalline basement, which comprises rock of the *Bamble and Kongsberg LUs* (e.g., Kristoffersen et al., 2014). Based on our study and that of Bast et al. (2014), these lithologies of the Sveconorwegian basement are possibly the primary source of the heavy B isotopic signature, at least as documented along the west side of the Oslo rift (Kragerø and Modum). Boron isotope data are not available from the Ordovician-Silurian sediments of the Oslo rift to confirm this model, but we suggest that isotopically heavy B is a regional, inherited signature related to an original marine-sedimentary component which has manifested itself in several episodes of orogeny and tourmaline formation since at least the Mesoproterozoic.

An anatectic origin for the investigated pegmatites was suggested previously by Müller et al., (2015,2017) and Rosing-Schow et al. (2023) based on the absence of coeval granites in the study areas, the generally low, initial fractionation degree of the pegmatite melt, the evidence for high-grade amphibolite-grade metamorphism, and macro and micro textures distinct for partial melting of host rocks at the time of pegmatite emplacement. The supposed anatectic origin is supported by the new tourmaline B-isotope data from the Lindvikskollen and Spro localities, where the same contrasting composition is shared by both pegmatites and their host rocks (Fig. 8). The similarity of whole-rock element distribution patterns of pegmatite and host rocks at Lindvikskollen (Fig. 4C) further suggests that the pegmatite melt was sourced by partial melting of rocks similar to those exposed at the surface. The situation is more complex at the Spro locality in the *Idefjorden LU*. Here, the $\delta^{11}B$ values of pegmatite and host rock tourmalines overlap but the Spro pegmatite and orthogneiss host rocks have different incompatible element and REE distribution patterns (Fig. 4E and F). Thus, the melt source at depth cannot be the same as the exposed host rocks but their respective B-isotope compositions must be similar. Since the Spro tourmaline $\delta^{11}B$ values overlap with the B-isotope ratio of the average upper crust, typical crustal orthogneisses or metasedimentary rocks at depth could be the source of the pegmatite melt (Fig. 8). In contrast to Lindvikskollen, the Spro pegmatite is situated in a vertical regional shear zone, which may have enabled the partial melts to travel farther and originate from a greater depth.

The NYF signature of the Lindvikskollen and other pegmatites in the Kragerø field, as defined by higher F and REE contents than typical metasediment-derived LCT pegmatites, can be explained if partial melting involved the breakdown of amphibole and biotite, and those are the most abundant hydrous phases in the host rocks of the pegmatites. Another important factor is likely to be the widespread Na-metasomatism in the Kragerø and Modum areas (Engvik et al., 2011; 2014), which caused local hydration of the high-grade metamorphic assemblages in permeable lithologies and along fault zones. This event was dated at 1110–1070 Ma (Munz et al., 1994; Engvik et al., 2017), shortly prior to pegmatite formation. The metasomatized, hydrated rocks will have lower melting temperature than unaltered rocks enhancing partial melting of metasomatized domains (Hansen et al., 2015; Beckmann et al., 2017). The fact that the Kragerø and Modum pegmatites occur preferentially in areas that underwent Na-metasomatism (Fig. 1) implies that the metasomatism may have controlled the regional distribution of pegmatites, in addition to imparting a distinctive, heavy B-isotope signature.

8. Conclusions

The key findings of this study and their significance are summarized as follows:

- The $\delta^{11}B$ values of tourmalines from the Sveconorwegian pegmatites of the *Bamble and Kongsberg Lithologic Units* (LU) are characterised by heavy B isotope signatures (−1.0 to + 9.9 ‰), typical for a marine-related B source, whereas tourmalines from the *Idefjorden LU* have typical crustal values (−14.8 ‰ to −12.5 ‰). Thus, B sources are different for pegmatites in different Sveconorwegian LUs.
- Boron isotopic compositions of tourmalines from different zones of one pegmatite, as illustrated for the Lindvikskollen locality, are nearly identical, indicating little B isotope fractionation within complexly- zoned NYF pegmatites.
- Tourmaline in host rocks near pegmatite contacts, which is interpreted to have crystallized from B-bearing aqueous fluids expelled from the crystallizing pegmatites, has overlapping $\delta^{11}B$ values with tourmaline from the parental pegmatites. This suggests that the magmatic-hydrothermal transition and fluid interaction with the host rock had little effect on the B isotopic signature.
- The heavy B-isotope signature observed in the *Bamble and Kongsberg LUs* was most likely inherited from the Na-metasomatised source rocks. Regional fluid plumes in these LUs, sourced from metamorphic dehydration of Mesoproterozoic shallow marine sediments at greater depth, caused hydration in permeable lithologies and along fault zones over large areas of the basement prior to pegmatite formation. We suggest that the marine source of hydration fluids caused the heavy B-isotope composition of pegmatite melts. Furthermore, the metasomatism enhanced partial melting of the affected rocks, which explains the preferential occurrence of Kragerø and Modum pegmatites in areas with Na-metasomatism (Fig. 1).
- The comparison of element distribution patterns in bulk rock pegmatite and host rock reveal their genetic relationships, a conclusion supported by the tourmaline chemical data. In the case of Lindvikskollen, trace element patterns of the pegmatite and metasomatised metagabbro are similar, implying that this lithology can be the melt source of the Lindvikskollen pegmatite at greater depth. The chemical NYF signature of the investigated pegmatites, defined by higher F and REE compared to metasediment-derived LCT pegmatite, suggests the breakdown of amphiboles and biotites during partial melting of the metagabbro.

Our findings document another important occurrence of tourmaline

in NYF-type pegmatites in addition to the handful that have recently been described. The implication is that tourmaline may be more common in, and boron enrichment may play a more significant role in the formation of, the NYF type pegmatites than previously believed. This study and others like it demonstrate that tourmaline can serve as a useful mineral for evaluating genetic models not just of the LCT pegmatites to which it has typically been applied, but to the NYF pegmatites as well.

CRediT authorship contribution statement

Erika De La Cruz: Writing – original draft, Visualization, Investigation, Formal analysis. **Axel Müller:** Writing – review & editing, Validation, Supervision, Conceptualization. **Robert B. Trumbull:** Writing – review & editing, Validation, Supervision, Methodology. **Pedro Faria:** Writing – review & editing, Investigation, Formal analysis. **Tom Andersen:** Writing – review & editing, Visualization, Supervision. **Muriel Erambert:** Writing – review & editing, Methodology. **Magnus Kristoffersen:** Writing – review & editing, Methodology.

Declaration of competing interest

The authors declare that they have no known competing financial interests or personal relationships that could have appeared to influence the work reported in this paper.

Data availability

Data will be made available on request.

Acknowledgements

We are very grateful to Alf Olav Larsen for his field assistance in the Kragerø area. We thank the reviewers Kathryn Goodenough and Øyvind Sunde for careful and constructive reviews and the editor Victoria Pease for thoughtful editorial handling.

Appendix A. Supplementary data

Supplementary data to this article can be found online at https://doi.org/10.1016/j.precamres.2024.107474.

References

Actlabs, 2023. Geochemistry. < https://actlabs.com/wp-content/uploads/2024/01/Actlabs-Geochemistry-Schedule-of-Services-2024-%E2%80%93-CAD.pdf> accessed 28 February 2023.
Åhäll, K.-I., Connelly, J.N., 2008. Long-term convergence along SW fennoscandia: 330 M. Y. of proterozoic crustal growth. Precambr. Res. 161, 452–474.
Anders, E., Grevesse, N., 1989. Abundances of the elements: Meteoritic and solar. Geochim. Cosmochim. Acta 53, 197–214.
Andersen, O., 1931. Feltspat II. Forekomster i fylkene Buskerud og Telemark, i flere herreder i Aust-Agder og i Hidra i Vest-Agder. Nor. Geol. Unders. 128b, 1–109.
Andersen, T., 1997. Radiogenic isotope systematics of the Herefoss granite, South Norway: an indicator of Sveconorwegian (Grenvillian) crustal evolution in the Baltic Shield. Chem. Geol. 135, 139–158.
Andersen, T., 2005. Terrane analysis, regional nomenclature and crustal evolution in the Southwest Scandinavian Domain of the Fennoscandian Shield. GFF 127, 159–168.
Andersen, T., Knudsen, T.-L., 1996. Precambrian crustal components in South Norway. Abstracts of the 22nd Nordic Geological Winter Meeting, Turku, Åbo, p. 12.
Andersen, T., Grorud, H.-F., 1998. Age and lead isotope systematics of uranium-enriched cobalt mineralization in the Modum complex, south Norway: implications for Precambrian crustal evolution in the SW part of the Baltic Shield. Precambr. Res. 91, 419–432.
Andersen, T., Maijer, C., Verschure, R.H., 1995. Metamorphism, provenance ages, and source characteristics of Precambrian clastic sediments in the Bamble sector, Southern Norway: Ar, Sr, Nd, and Pb isotopic study. Petrology (moscow) 3, 321–339.
Andersen, T., Andresen, A., Sylvester, A.G., 2001. Nature and distribution of deep crustal reservoirs in the southwestern part of the Baltic Shield: Evidence from Nd, Sr and Pb isotope data on late Sveconorwegian granites. J. Geol. Soc. 158, 253–267.
Andersen, T., Griffin, W.L., Jackson, S.E., Knudsen, T.L., Pearson, N.J., 2004. Mid-Proterozoic magmatic arc evolution at the southwest margin of the Baltic Shield. Lithos 73, 289–318.
Andersen, T., Sylvester, A.G., Graham, S., 2007. Timing and tectonic significance of Sveconorwegian A-type granitic magmatism in Telemark, southern Norway: New results from laser-ablation ICPMS U-Pb dating of zircon. NGU Bull. 447, 17–31.
Barth, S., 1993. Boron isotope variations in nature: a synthesis. Geol. Rundsch. 82, 640–651.
Bast, R., Scherer, E.E., Mezger, K., Austrheim, H., Ludwig, T., Marschall, H.R., Putnis, A., Löwen, K., 2014. Boron isotopes in tourmaline as a tracer of metasomatic processes in the Bamble sector of Southern Norway. Contrib. Miner. Petrol. 168, 1069.
Beckmann, V., Möller, C., Söderlund, U., Andersson, J., 2017. Zircon growth during progressive metamorphic recrystallization of gabbro to garnet amphibolite, Eastern Segment, Sveconorwegian orogen. J. Petrol. 58, 167–187.
Beurlen, H., De Moura, O.J., Soares, D.R., Da Silva, M.R., Rhede, D., 2011. Geochemical and geological controls on the genesis of gem-quality "Paraíba Tourmaline" in granitic pegmatites from northeastern Brazil. Can. Mineral. 49, 277–300.
Bingen, B., Birkeland, A., Nordgulen, Ø., Sigmond, E.M.O., 2001. Correlation of supracrustal sequences and origin of terranes in the Sveconorwegian orogen of SW Scandinavia: SIMS data on zircon in clastic metasediments. Precambr. Res. 108, 293–318.
Bingen, B., Nordgulen, O., Viola, G., 2008. A four-phase model for the Sveconorwegian orogeny, SW Scandinavia. NGT 88, 43–72.
Bingen, B., Viola, G., Möller, C., Vander Auwera; J., Laurent, A., Yi, K.,, 2021. The Sveconorwegian orogeny. Gondwana Res. 90, 273–313.
Breaks, F.W., Selway, J.B., Tindle, A.G., 2003. Fertile peraluminous granites and related rare-element mineralization in pegmatites, Superior Province, northwest and northeast Ontario: Operation Treasure Hunt. Ontario Geol, Surv, p. 179.
Brenan, J.M., Ryerson, F.J., Shaw, H.F., 1998. The role of aqueous fluids in the slab-to-mantle transfer of boron, beryllium, and lithium during subduction: experiments and models. Geochim. Cosmochim. Acta 62, 3337–3347.
Brøgger, W., 1903. Über der Hellandit, ein neues Mineral. Nyt Magazin for Naturvidenska Berne Kristainia 41, 213–221.
Bugge, A., 1965. Iakttagelser fra rektangelbladet Kragerø og den store grunnfjellsbreksje. NGU Nr. 229.
Bugge, A., 1955. Befaring av Spro feltspatforekomst, Nesodden, Akershus. NGU Report No.BA 6205, 2.
Catanzaro, E.J., 1970. Boric acid: isotopic and assay standard reference materials. Mater. Res, National Bureau of Standards, Inst.
Černý, P., London, D., Novák, M., 2012. Granitic pegmatites as reflections of their sources. Elements 8, 289–294.
Cheng, L., Zhang, C., Zhou, Y., Horn, I., Weyer, S., Holtz, F., 2022. Experiments reveal enrichment of 11B in granitic melt resulting from tourmaline crystallization. Geochem Persp. Let. 20, 37–42.
De Haas, G.X., Jan, L.M., Andersen, T., Vestin, J., 1999. Detrital zircon geochronology: New evidence for an old model for accretion of the southwest Baltic Shield. J. Geol. 107, 569–586.
De Haas, G.-J.-L.-M., Verschure, R.H., Maijer, C., 1993. Isotopic constraints on the timing of crustal accretion of the Bamble Sector, Norway, as evidenced by coronitic gabbros. Precambr. Res. 64, 403–417.
De Hoog, J.C.M., Savov, I.P., 2018. Boron isotopes as a tracer of subduction zone processes. In: Marschall, H., Foster, G. (Eds.), Boron Isotopes Advances in Isotope Geochemistry, 9th ed. Springer International Publishing, Berlin, pp. 217–247.
De la Cruz, E., 2021. Tourmaline of the Kragerø pegmatites. The source of boron and its implication for the melt formation of Sveconorwegian pegmatites. Natural History Museum, University of Oslo, Oslo <https://www.duo.uio.no/handle/10852/88422>. MSc thesis.
De la Cruz, E., Müller, A., Erambert, M., 2021. The Lindvikskollen pegmatite at Kragerø: New mapping and mineral chemistry results. In: Larsen A.O., Kjærnet T., eds., Norsk Mineralsymposium 2021, 61-70.
De la Roche, H., Leterrier, J., Grandclaude, P., Marchal, M., 1980. A classification of volcanic and plutonic rocks using R1R2-diagram and major-element analyses - Its relationships with current nomenclature. Chem. Geol. 29, 183–210.
Elliott, R.B., 1966. The Association of Amphibolite and Albitite, Kragerø, South Norway. Geol. Mag. 103, 1–7.
Engvik, A.K., Putnis, A., Fitz Gerald, J., Austrheim, H., 2008. Albitization of granitic rocks: The mechanism of replacement of oligoclase by albite. Can. Mineral. 46, 1401–1415.
Engvik, A.K., Golla-Schindler, U., Berndt, J., Austrheim, H., Putnis, A., 2009. Intragranular replacement of chlorapatite by hydroxy-fluor-apatite during metasomatism. Lithos 112, 236–246.
Engvik, A.K., Mezger, K., Wortelkamp, S., Bast, R., Corfu, F., Korneliussen, A., Ihlen, P., Bingen, B., Austrheim, H., 2011. Metasomatism of gabbro – mineral replacement and element mobilization during the Sveconorwegian metamorphic event. J. Metam. Geol. 29, 399–423.
Engvik, A.K., Ihlen, P.M., Austrheim, H., 2014. Characterisation of Na-metasomatism in the Sveconorwegian Bamble Sector of South Norway. Geosci. Front. 5, 659–672.
Engvik, A.K., Corfu, F., Solli, A., Austrheim, H., 2017. Sequence and timing of mineral replacement reactions during albitisation in the high-grade Bamble lithotectonic domain. S-Norway. Precambr. Res. 291, 1–16.
Engvik, A.K., Taubald, H., Solli, A., Grenne, T., Austrheim, H., 2018. Dynamic metasomatism: stable isotopes, fluid evolution, and deformation of albitite and scapolite metagabbro (Bamble lithotectonic domain. South Norway), Geofluids, p. 2018.
Faria, P., 2019. The mineralogy and chemistry of the Spro pegmatite mine, Nesodden, and their genetic implications. University of Oslo. MSc thesis.
Frost, B.R., Frost, C.D., 2008. A geochemical classification for feldspathic igneous rocks. J. Petrol. 49, 1955–1969.

Granseth, A., Slagstad, T., Coint, N., Roberts, N.M.W., Røhr, T.S., Sørensen, B.E., 2020. Tectonomagmatic evolution of the Sveconorwegian orogen recorded in the chemical and isotopic compositions of 1070–920 Ma granitoids. Precambr. Res. 340, 105527.
Green, J.C., 1956. Geology of the Storkollen-Blankenberg area, Kragerø, Norway. NGT 36, 89–140.
Griffin, W., 2008. GLITTER: data reduction software for laser ablation ICP-MS. Laser Ablation ICP-MS in the Earth Sciences: Current practices and outstanding issues, 308-311.
Hansen, E., Johansson, L., Andersson, J., LaBarge, L., Harlov, D., Möller, C., Vincent, S., 2015. Partial melting in amphibolites in a deep section of the Sveconorwegian Orogen, SW Sweden. Lithos 236, 27–45.
Heaman, L.M., Smalley, P.C., 1994. A U-Pb study of the Morkheia Complex and associated gneisses, southern Norway: implications for disturbed Rb-Sr systems and for the temporal evolution of Mesoproterozoic magmatism in Laurentia. Geochim. Cosmochim. Acta 58, 1899–1911.
Henry, D.J., Guidotti, C.V., 1985. Tourmaline as a petrogenetic indicator mineral – an example from the staurolite-grade metapelites of NW Maine. Am. Mineral. 70, 1–15.
Henry, D.J., NováK, M., Hawthorne, F.C., Ertl, A., Dutrow, B.L., Uher, P., Pezzotta, F., 2011. Nomenclature of the tourmaline-supergroup minerals. Am. Mineral. 96, 895–913.
Høy, I.U., 2016. Sveconorwegian magmatic and metamorphic evolution of southwestern Norway. Univeristy of Oslo. MSc thesis.
Jacobsen, S.B., Heier, K.S., 1978. Rb-Sr isotope systematics in metamorphic rocks, Kongsberg sector, south Norway. Lithos 11, 257–276.
Jahns, R. H. 1955. The study of pegmatites. Econ. Geol., 50th Anniv. Vol., 1905-1955, 1025-1130.
Jensen, E., Corfu, F., 2016. The U-Pb age of the Finse batholith, a composite bimodal Sveconorwegian intrusion. Norw. J. Geol. 96, 171–178.
Jøsang, O., 1966. Geologiske og petrografiske undersøkelser i Modumfeltet. NGU. Bulletin of the Georgian Academy of Sciences 235.
Knoll, T., Huet, B., Schuster, R., Mali, H., Ntaflos, T., Hauzenberger, C., 2023. Lithium pegmatite of anatectic origin - a case study from the Austroalpine Unit Pegmatite Province (eastern European Alps): geological data and geochemical model. Ore Geol. Rev. 154, 105298.
Knudsen, T.L., Andersen, T., Whitehouse, M.J., Vestin, J., 1997. Detrital zircon ages from southern Norway – implications for the Proterozoic evolution of the southwestern Baltic Shield. Contrib. Mineral. Petrol. 130, 47–58.
Konrad-Schmolke, M., Halama, R., 2014. Combined thermodynamic-geochemical modeling in metamorphic geology: boron as tracer of fluid–rock interaction. Lithos 208, 393–414.
Kowalski, P., Wunder, B., 2018. Boron isotope fractionation among vapor-liquids-solids-melts: experiments and atomistic modelling. In: Marschall, H.R., Foster, G.L. (Eds) Boron Isotopes - The Fifth Element. Advances in Geochemistry, vol. 7, Springer, Heidelberg, 33-69.
Kristiansen, R., 1993. Caysichitt-(Y) og Chernovitt-(Y) fra Lindvikskollen, Kragerø; to nye mineraler for Norge. Stein 20, 125–128.
Kristoffersen, M., Andersen, T., Andresen, A., 2014. U-Pb age and Lu-Hf signatures of detrital zircon from Palaeozoic sandstones in the Oslo Rift. Norway. Geol. Mag. 151, 816–829.
Larsen, K.E., 2008. Lindvikskollen-Kalstadgangen, Kragerø- en klassisk norsk granittpegmatitt. Norsk Bergverksmuseum Skrift 38, 37–44.
Leeman, W.P., Tonarini, S., 2001. Boron isotopic analysis of proposed borosilicate mineral reference samples. Geostand. Geoanl. Res. 25, 399–403.
Lieftink, D.J., Nijland, T.G., Maijer, C., 1994. The behavior of rare-earth elements in high-temperature Cl-bearing aqueous fluids: results from the Ødegårdens Verk natural laboratory. Can. Mineral. 32, 149–158.
Marschall, H.R., Altherr, R., Rüpke, L., 2007. Squeezing out the slab — modelling the release of Li, Be and B during progressive high-pressure metamorphism. Chem. Geol. 239, 323–335.
Marschall, H., Jiang, S.-Y., 2011. Tourmaline isotopes: No element left behind. Elements 7, 313–319.
Marschall, H.R., Korsakov, A.V., Luvizotto, G.L., Nasdala, L., Ludwig, T., 2009. On the occurrence and boron isotopic composition of tourmaline in (ultra)high-pressure metamorphic rocks. J. Geol. Soc. 166, 811–823.
Marschall, H.R., 2018. Boron isotopes in the ocean floor realm and the mantle. In: Marschall, H., Foster, G., eds., Boron Isotopes, Advances in Isotope Geochemistry. Springer International Publishing AG 2018, 189-215.
Meyer, C., Wunder, B., Meixner, A., Romer, R.L., Heinrich, W., 2008. Boron-isotope fractionation between tourmaline and fluid: an experimental re-investigation. Contrib. Mineral. Petrol. 156, 259–267.
Möller, C., Andersson, J., Dyck, B., Antal Lundin, I., 2015. Exhumation of an eclogite terrane as a hot migmatitic nappe, Sveconorwegian orogen. Lithos 226, 147–168.
Moran, A.E., Sisson, V.B., Leeman, W.P., 1992. Boron depletion during progressive metamorphism: implications for subduction processes. Earth Planet. Sci. Lett. 111, 331–349.
Müller, A., Ihlen, P.M., Snook, B., Larsen, R.B., Flem, B., Bingen, B., Williamson, B.J., 2015. The chemistry of quartz in granitic pegmatites of southern Norway: Petrogenetic and economic implications. Econ. Geol. 110, 1737–1757.
Müller, A., Romer, R., Pedersen, R.-B., 2017. The Sveconorwegian Pegmatite Province – Thousands of Pegmatites Without Parental Granites. Can. Mineral. 55, 283–315.
Müller, A., Simmons, W., Beurlen, H., Thomas, R., Wise, I.P.M., M., Roda-Robles, E., Neiva, A.M.R., Zagorsky, V.,, 2022. A proposed new mineralogical classification system for granitic pegmatites – Part I: History and the need for a new classification. Can. Mineral. 60, 203–227.
Munz, I.A., 1990. Whiteschists and orthoamphibole-cordierite rocks and the P-T-t path of the Modum Complex, south Norway. Lithos 24, 181–199.
Munz, I.A., Wayne, D., Austrheim, H., 1994. Retrograde fluid infiltration in the high-grade Modum Complex South Norway: evidence for age, source and REE mobility. Contrib. Mineral. Petrol. 116, 32–46.
Munz, I.A., Yardley, B.W.D., Banks, D.A., Wayne, D., 1995. Deep penetration of sedimentary fluids in basement rocks from southern Norway: Evidence from hydrocarbon and brine inclusions in quartz veins. Geochim. Cosmochim. Acta 59, 239–254.
Narum, M.N., Gabrielsen, R.H., Corfu, F., 2021. Tectonometamorphic history of the Østfold Gneiss Complex, Idefjorden lithotectonic unit, southeastern Norway. Nor. J. Geol. 101, 202117.
Nijland, T.G., Touret, J., 2001. Replacement of graphic pegmatite by graphic albite-actinoliteclinopyroxene intergrowths (Mjåvatn, southern Norway). Eur. J. Mineral. 13, 41–50.
Nijland, T.G., Harlov, D.E., Andersen, T., 2014. The Bamble Sector, South Norway: A review. Geosci. Front. 5, 635–658.
Novák, M., Škoda, R., Filip, J., Macek, I., Vaculovič, T., 2011. Compositional trends in tourmaline from intragranitic NYF pegmatites of the Trebic pluton, Czech Republic: an electron microprobe, Mössbauer and LA-ICP-MS study. Can. Mineral. 49, 359–380.
Palmer, M.R.P., 2017. Boron cycling in subduction zones. Elements 13, 237–242.
Pedersen, S., Berthelsen, A., Falkum, T., Graversen, B., Hageskov, B., Malloe, S., 1978. Rb/Sr-dating of the plutonic and tectonic evolution of the Sveconorwegian Province, southern Norway. USGS Open File Report 78–701, 329–331.
Pouchou, J.L., Pichoir, F., 1984. A new model for quantitative X-ray microanalysis. I. Application to the analysis of homogenous samples. Rech. Aèrospat. 3, 13–38.
Pózer Bue, E., 2008. Age and origin of the Mesoproterozoic basement of the Nesodden Peninsula, SE Norway: A geochronological and isotopic study. University of Oslo. MSc Master thesis,.
Raade, G., 1965. The minerals of the granite pegmatite at Spro, Nesodden, near Oslo. NGU Nr. 234.
Ribacki, E., Trumbull, R.B., Lopez de Luchi, M.G., Altenberger, U., 2022. The chemical and B-isotope composition of tourmaline from intra-granitic pegmatites in the Las Chacras-Potrerillos Batholith. Argentina. Can. Mineral. 60, 49–66.
Roberts, N.M.W., Slagstad, T., Parrish, R.R., Norry, M.J., Marker, M., Horstwood, M.S.A., 2013. Sedimentary recycling in arc magmas: geochemical and U-Pb–Hf–O constraints on the Mesoproterozoic Suldal Arc, SW Norway. Contrib. Mineral. Petrol. 165, 507–523.
Roda-Robles, E., Simmons, W., Pesquera, A., Gil-Crespo, P.P., Nizamoff, J., Torres-Ruiz, J., 2015. Tourmaline as a petrogenetic monitor of the origin and evolution of the Berry-Havey pegmatite (Maine, U.S.A.). Am. Mineral. 100, 95–109.
Rosing-Schow, N., Romer, R.L., Müller, A., Corfu, F., Škoda, R., Friis, H., 2023. Geochronological constraints for a two-stage history of the Sveconorwegian rare-element pegmatite province formation. Precambr. Res. 384, 106944.
Rudnick, R., Gao, S., 2003. Composition of the continental crust. The Crust 3, 1–64.
Sanchez-Valle, C., Reynard, B., Daniel, I., Lecuyer, C., Martinez, I., Chervin, J.C., 2005. Boron isotopic fractionation between minerals and fluids: new insights from in situ high pressure–high temperature vibrational spectroscopic data. Geochim. Cosmochim. Acta 69, 4301–4313.
Schei, P., 1904. On some new occurrences of titanite from Kragerø. Nyt Magazin for Naturvidenskaberne 42, 35–38.
Shaw, R.A., Goodenough, K.M., Roberts, N.M.W., Horstwood, M.S.A., Chenery, S.R., Gunn, A.G., 2016. Petrogenesis of rare-metal pegmatites in high-grade metamorphic terranes: A case study from the Lewisian Gneiss Complex of north-west Scotland. Precambr. Res. 281, 338–436.
Simmons, W., Falster, A., Webber, K., Roda-Robles, E., Boudreaux, A.P., Grassi, L.R., Freeman, G., 2016. Bulk composition of Mt. Mica pegmatite, Maine, USA: Implications for the origin of an LCT type pegmatite by anatexis. Can. Mineral. 54, 1053–1070.
Skiöld, T., 1976. The interpretation of the Rb-Sr and K-Ar ages of late Precambrian rocks in south-western Sweden. GFF 98, 3–29.
Slagstad, T., Roberts, N.M.W., Marker, M., Røhr, T.S., Schiellerup, H., 2012. A non-collisional, accretionary Sveconorwegian orogen. Terra Nova 25, 30–37.
Slagstad, T., Roberts, N.M.W., Kulakov, E., 2017. Linking orogenesis across a supercontinent; the Grenvillian and Sveconorwegian margins on Rodinia. Gondwana Res. 44, 109–115.
Slagstad, T., Marker, M., Roberts, N.M.W., Saalmann, K., Kirkland, C.L., Kulakov, E., Ganerød, M., Røhr, T.S., Møkkelgjerd, S.H.H., Granseth, A., Sørensen, B.E., 2020. The Sveconorwegian orogeny – Reamalgamation of the fragmented southwestern margin of Fennoscandia. Precambr. Res. 350, 105877.
Söderlund, U., Isachsen, C.E., Bylund, G., Heaman, L.M., Jonathan Patchett, P., Vervoort, J.D., Andersson, U.B., 2005. U-Pb baddeleyite ages and Hf, Nd isotope chemistry constraining repeated mafic magmatism in the Fennoscandian Shield from 1.6 to 0.9 Ga. Contrib. Mineral. Petrol. 150, 174–194.
Starmer, I.C., 1985. The evolution of the south Norwegian Proterozoic as revealed by major and mega-tectonics of the Kongsberg and Bamble sectors. In: Tobi, A.C., Touret, J.L.R. (Eds.), The Deep Proterozoic Crust in the North Atlantic Provinces. Reidel, Dordrecht.
Sunde, Ø., Friis, H., Andersen, T., Trumbull, R.B., Wiedenbeck, M., Lyckberg, P., Agostini, S., Casey, W.H., Yu, P., 2020. Boron isotope composition of coexisting tourmaline and hambergite in alkaline and granitic pegmatites. Lithos 352–353, 105293.
Torgersen, E., Arntsen, M.L., Bingen, B., Gasser, D., Gunleiksrud, I.H., Nilsson, C., et al., 2021. Bedrock map of Norway, 1:1350000. NGU, Trondheim, Norway.
Trumbull, R. B., Slack, J. F., 2018. Boron isotopes in the continental crust: granites, pegmatites, felsic volcanic rocks, and related ore deposits. In: Marschall, H.R.,

Foster, G.L. (Eds) Boron Isotopes - The Fifth Element. Advances in Geochemistry, vol. 7, Springer, Heidelberg, 249-272.
Van der Auwera, J., Bolle, O., Bingen, B., Liégeois, J.P., Bogaerts, M., Duchesne, J.C., De Waele, B., Longhi, J., 2011. Sveconorwegian massif-type anorthosites and related granitoids result from post-collisional melting of a continental arc root. Earth Sci. Rev. 107, 375–397.
Van Hinsberg, V., Henry, D.J., Marschall, H., 2011a. Tourmaline: An ideal indicator of its host environment. Can. Mineral. 49, 1–16.
Van Hinsberg, V.J., Henry, D.J., Dutrow, B.L., 2011b. Tourmaline as a petrologic forensic mineral: A unique recorder of its geologic past. Elements 7, 327–332.
Veritas, B., 2023. Mining laboratory services. Accessed 28 February 2023. <https://www.bvna.com/other-markets/mining-laboratory-services>.
Viola, G., Bingen, B. Henderson, I., Yi, K., Ganerød, M., 2013. The Kongsberg-Modum terrane of Southern Norway: a key toward a refined conceptual model of the Sveconorwegian orogeny. Geophysical Research Abstracts, Vol. 15, EGU General Assembly 2013, EGU2013-10323, 2013.
Viola, G., Bingen, B., Solli, A., 2016. Berggrunnskart: Kongsberg litotektoniske enhet, Kongsberg - Modum - Hønefoss M 1:100 000. NGU Trondheim.
Whalen, J.B., Currie, K.L., Chappell, B.W., 1987. A-type granites: geochemical characteristics, discrimination and petrogenesis. Contrib. Mineral. Petrol. 95, 405–419.
Wise, M., 1999. Characterization and classification of NYF type pegmatites. Can. Mineral. 37, 802–803.
Zhou, Q., Li, W., Wang, G., Liu, Z., Lai, Y., Huang, J., Yan, G., Zhang, Q., 2021. Chemical and boron isotopic composition of tourmaline from the Conadong leucogranite-pegmatite system in South Tibet. Lithos 326–327, 529–539.